Available online at www.sciencedirect.com
ScienceDirect
Journal of Sound and Vibration 308 (2007) 302–329
JOURNAL OF SOUND AND VIBRATION
www.elsevier.com/locate/jsvi

Dynamics of a hypoid gear pair considering the effects of time-varying mesh parameters and backlash nonlinearity

Jun Wang, Teik C. Lim*, Mingfeng Li

Mechanical Engineering, 598 Rhodes Hall, P.O. Box 210072, University of Cincinnati, Cincinnati, OH 45221, USA

Received 4 January 2007; received in revised form 22 May 2007; accepted 26 July 2007
Available online 4 September 2007

Abstract

A generalized nonlinear time-varying (NLTV) dynamic model of a hypoid gear pair with backlash nonlinearity is formulated which is also applicable to spur, helical, spiral bevel and worm gears. Firstly, the fundamental harmonic form of time-varying mesh parameters is used to study the effects of mesh parameter variations on the dynamic response, and the interactions between them and backlash nonlinearity. The analysis also examines the effects of mean load and mesh damping. Secondly, based on a three-dimensional quasi-static tooth contact analysis, a new significantly more exact time-varying mesh model is proposed, which describes the true mesh characteristics of hypoid gear pairs. The enhanced time-varying mesh model is applied to perform further dynamic analysis. Computational results reveal numerous interesting nonlinear characteristics, such as jump discontinuities, sub-harmonic and chaotic behaviors, especially for lightly loaded and lightly damped cases.

1. Introduction

Gear pair dynamics is one of the most important factors affecting the noise, vibration and durability performances of gearboxes, drivetrains and power transmission systems. Owing to the high sensitivity of the gear pair to its tooth profile errors, shaft misalignment, and overall structural dynamics, the vibratory response can be very complex and not easy to control. Therefore, gaining a more thorough understanding of the underlying physics governing the gear pair dynamics is essential in the design and development of quieter and more durable geared rotor systems. In this paper, we focus mainly on the dynamics of high-speed, precision hypoid gear pairs often used in automotive and aerospace power transmission systems.

Although parallel axis gear dynamics has been studied extensively [1–7], limited investigations [8–12] can be found on the dynamics of non-parallel axis gears such as hypoid and bevel gears on account of the complexity of gear kinematics and meshing characteristics. Most of the models on hypoid gear dynamics are limited to experimental or simple, semi-analytical formulation, and the effects of time-varying mesh characteristics are either not considered or only approximately represented. Remmers [8] studied the mass-elastic model of rear axle gears with infinite mesh stiffness to predict the pinion resonance and carried out experiments to confirm

*Corresponding author. Tel.: +1 513 556 4450; fax: +1 513 556 3390.
E-mail address: teik.lim@uc.edu (T.C. Lim).

0022-460X/$ - see front matter © 2007 Elsevier Ltd. All rights reserved.
doi:10.1016/j.jsv.2007.07.042

Nomenclature

b	gear backlash
c_m	mesh damping coefficient
e	kinematic transmission error
f	nonlinear displacement function
I_p, I_g	mass moments of inertias of pinion and gear
$\vec{j}_l$	unit vector along pinion/gear rotating axis
k, k_m	mesh stiffness
m_e	equivalent mass
$\vec{n}_l$	unit normal vector of mesh point
p	difference between dynamic transmission error and kinematic transmission error
$\vec{r}_l$	position vector of mesh point
S_l	coordinate system for dynamic formulation
t	time
T_p, T_g	mean load torques on pinion and gear
δ	dynamic transmission error
η	system parameter
λ_l	directional rotation radius
ξ	mesh damping ratio
ϕ	phase angle
ω	excitation frequency

Subscripts

l	label for pinion ($l = p$) and gear ($l = g$)
$a1$	fundamental harmonic
m	mean
n	natural

Superscripts

$\sim$	dimensionless quantities
$\rightarrow$	vector quantities
$'$	derivative with respect to time

the vibration peaks. Kiyono et al. [9] derived a two degrees-of-freedom (dofs) vibration model of a pair of bevel gears in which the line-of-action vector was simulated by a sine curve, and applied the model to conduct a stability analysis. Abe and Hagiwara [10] found that axle gear noise could be reduced by modifying the vibration mode with the addition of an inertia disk that can be mounted on either of the side flanges of the final drive in their experiment. Hirasaka et al. [11] proposed an experimental method to study the body and driveline sensitivity to unit transmission error of an axle hypoid gear pair. They estimated the force at the contact points of the gears, and found that the dynamic mesh force was affected by the torsional vibration characteristics of the driveline. Donley et al. [12] developed a dynamic model of a hypoid gear set for use in finite element analysis of gearing systems. In their gear mesh model, the mesh point and line-of-action are time invariant. More recently, Cheng and Lim [13–17] proposed a hypoid gear kinematic model based on exact gear geometry for analyzing gear mesh mechanism and applied the corresponding linear dynamic model to study the hypoid gear pair dynamics with transmission error excitation. They also studied the dynamics of hypoid gear transmission with NLTV mesh characteristics. Later Jiang and Lim [18] derived a NLTV dynamic model of a hypoid gear pair to investigate geared system response. They described the mesh parameters, typically represented by transmission error, contact stiffness, line-of-action and contact point, in the form of

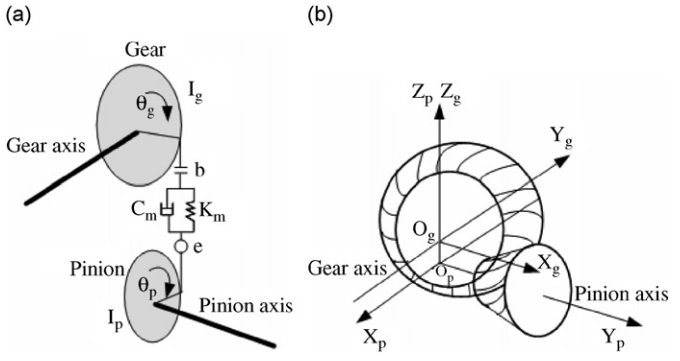

Fig. 1. (a) Torsional vibration model of a hypoid gear pair and (b) coordinate systems for pinion and gear.

fundamental harmonic that is a perfect sinusoid. Wang and Lim [19] developed a multipoint mesh model and applied it to analyze the hypoid gear dynamics. In all of Cheng, Jiang and Wang's publications, the time-dependent mesh parameters are expressed in the form of either fundamental harmonic or the first few harmonics.

In the present study, a general nonlinear time-varying (NLTV) dynamic model of a hypoid gear pair with backlash nonlinearity is proposed, which is also applicable to spur, helical, spiral bevel and worm gears even though that is not the primary focus of this investigation. Firstly, the fundamental harmonic form of gear mesh parameters similar to earlier work described above is used to study the effects of mesh parameter variations on dynamic response and the interactions between them and backlash nonlinearity. Here, the effects of mesh stiffness variation, pinion and gear directional rotation radius variation and kinematic transmission error variation are investigated. The analysis also examines the effects of mean load and mesh damping. Then, unlike the harmonic form previously used, a new significantly more exact time-varying gear mesh model is proposed and applied to further dynamic analysis. The new mesh coupling formulation is capable of describing the true hypoid gear tooth contact characteristics, which is expected to yield more refined prediction of dynamic response.

2. Mathematical model

The proposed generalized lumped parameter torsional vibration model of a hypoid gear is shown in Fig. 1(a). In theory, this concept is also applicable to spur, helical, spiral bevel and worm gears as long as the geometrical configuration is represented appropriately. Pinion and gear are modeled as rigid bodies with rotational displacements as their coordinates. Gear mesh is simulated by a pair of stiffness and damping elements along the line-of-action direction. Backlash nonlinearity and kinematic (also known as unloaded static) transmission error are also included.

From the proposed concept, the equations of motion of the two dof torsional vibration model can be derived as

$$I_p\ddot{\theta}_p + \lambda_p c_m(\dot{\delta} - \dot{e}) + \lambda_p k_m f(\delta - e) = T_p, \tag{1a}$$

$$I_g\ddot{\theta}_g - \lambda_g c_m(\dot{\delta} - \dot{e}) - \lambda_g k_m f(\delta - e) = -T_g, \tag{1b}$$

where I_p and I_g are mass moments of inertias of pinion and gear, T_p and T_g are mean load torques on pinion and gear, k_m is mesh stiffness, c_m is mesh damping coefficient, $f(\delta-e)$ is a nonlinear displacement function of the dynamic transmission error δ and kinematic transmission error e. The dynamic transmission error δ is defined as

$$\delta = \lambda_p\theta_p - \lambda_g\theta_g, \tag{2}$$

while the nonlinear displacement function $f(\delta-e)$ is given by

$$f(\delta - e) = \begin{cases} \delta - e - b, & \delta - e \geqslant b, \\ 0, & -b < \delta - e < b, \\ \delta - e + b, & \delta - e \leqslant -b, \end{cases} \tag{3}$$

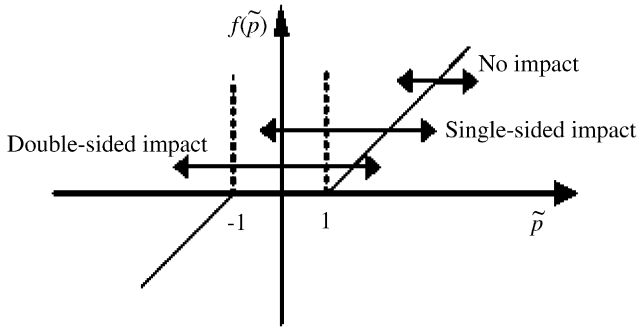

Fig. 2. Dimensionless nonlinear displacement function.

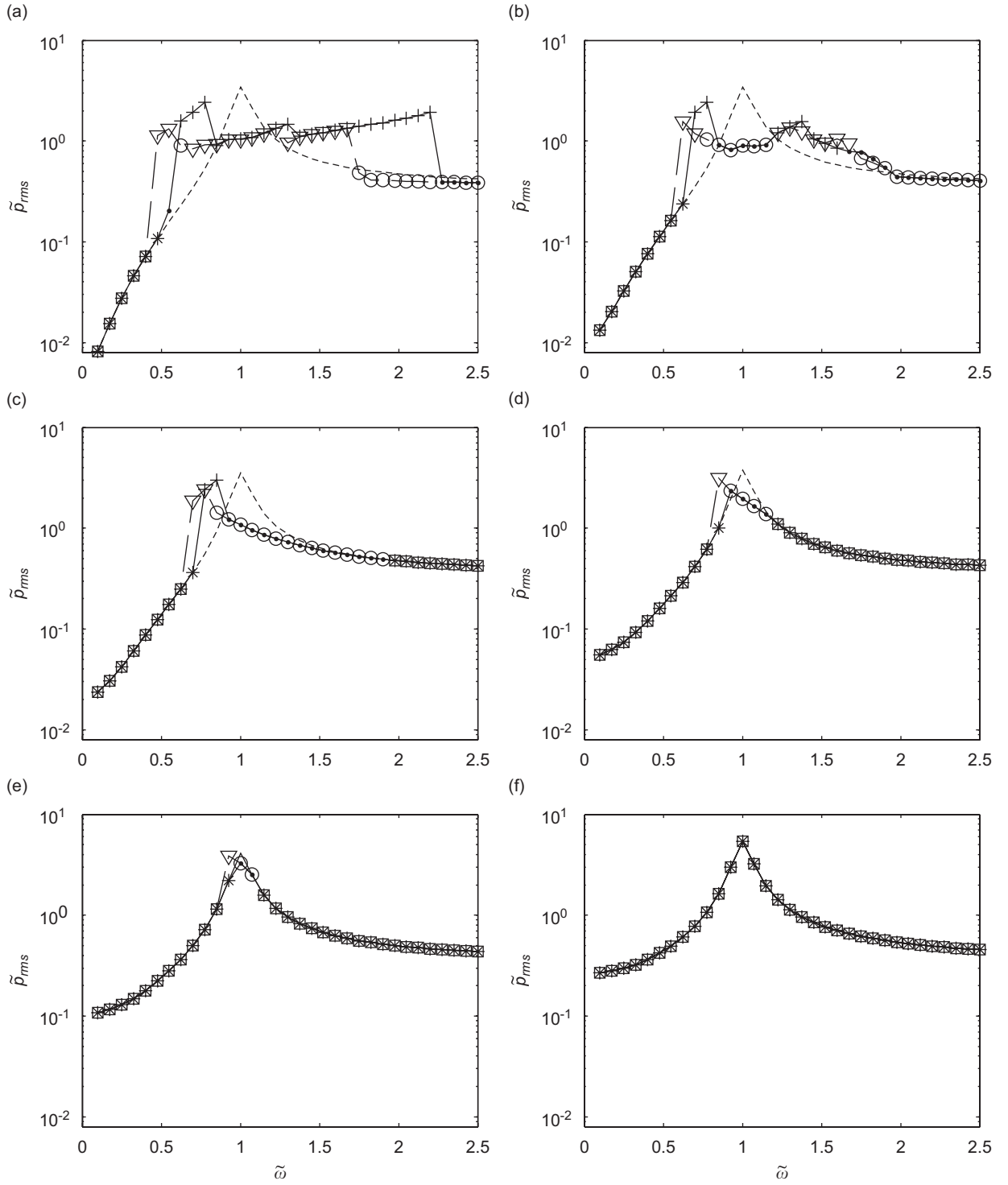

Fig. 3. Effect of mean load on frequency response: (a) $\tilde{T}_p = 0.1$; (b) $\tilde{T}_p = 0.2$; (c) $\tilde{T}_p = 0.4$; (d) $\tilde{T}_p = 1.0$; (e) $\tilde{T}_p = 2.0$; (f) $\tilde{T}_p = 5.0$; ∗, □ no impact; ●, ○ single-sided impact; +, ▽ double-sided impact; ———, NLTV (increasing frequency); ----------, NLTV (decreasing frequency); · · · · · · · · · · · , LTV.

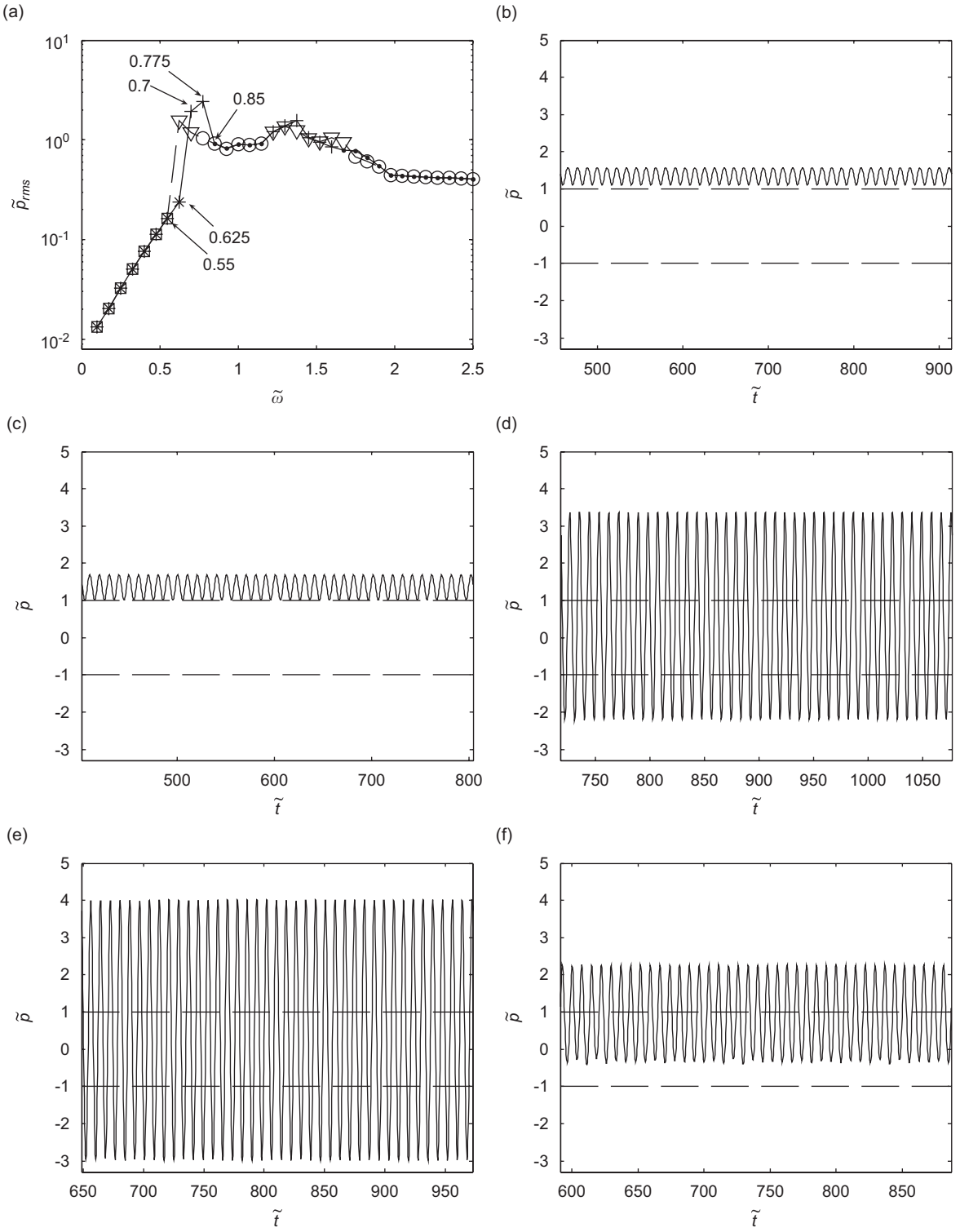

Fig. 4. Typical frequency response and time history plots: (a) Frequency response for $\tilde{T}_p = 0.2$; (b) time history at $\tilde{\omega} = 0.55$; (c) time history at $\tilde{\omega} = 0.625$; (d) time history at $\tilde{\omega} = 0.7$; (e) time history at $\tilde{\omega} = 0.775$; (f) time history at $\tilde{\omega} = 0.85$.

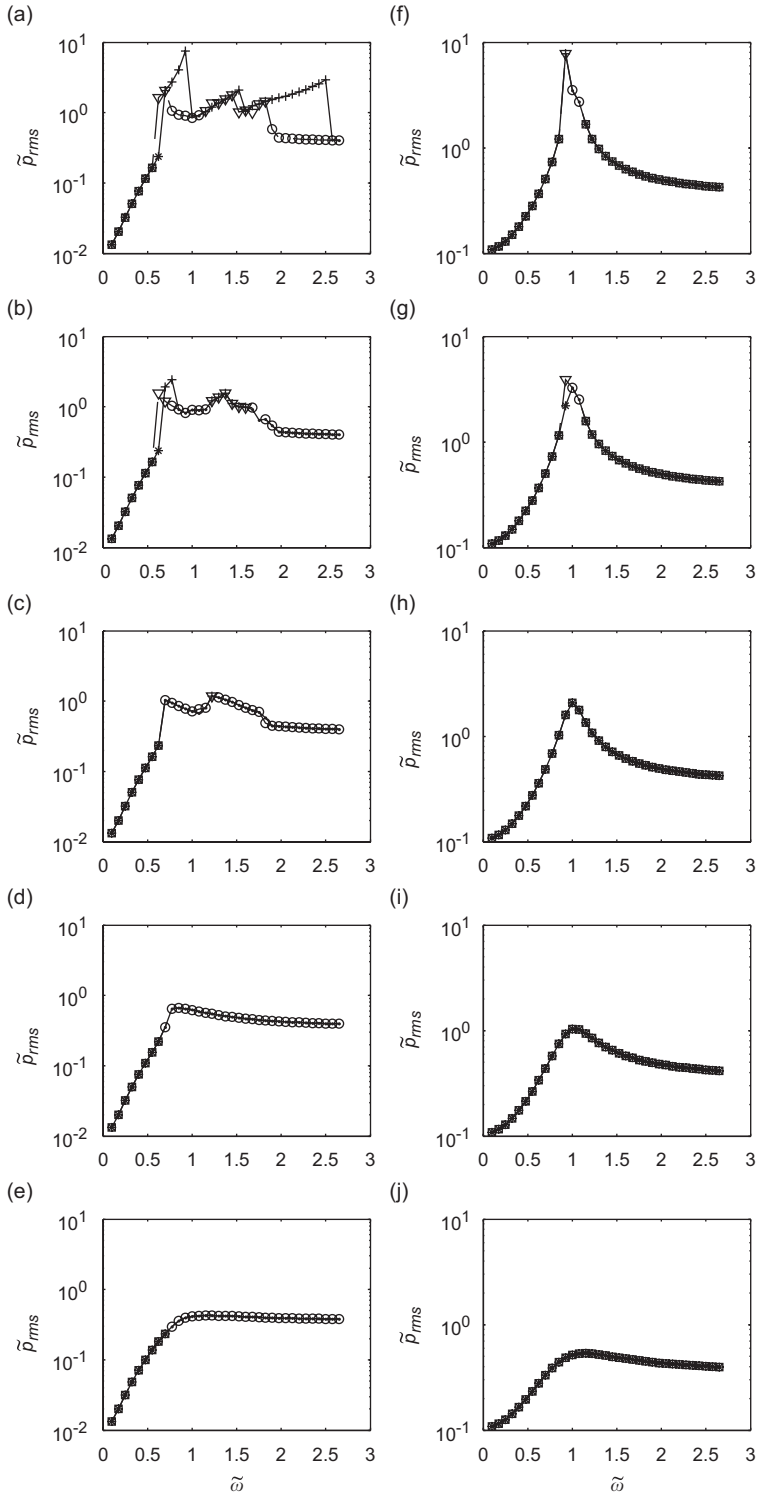

Fig. 5. Effect of mesh damping on frequency response. Lightly loaded case: $\tilde{T}_p = 0.2$, (a) $\xi = 0.01$, (b) $\xi = 0.03$, (c) $\xi = 0.06$, (d) $\xi = 0.12$, (e) $\xi = 0.24$. Heavily loaded case: $\tilde{T}_p = 2$, (f) $\xi = 0.01$; (g) $\xi = 0.03$; (h) $\xi = 0.06$; (i) $\xi = 0.12$; (j) $\xi = 0.24$. ∗, □ no impact; ●, ○ single-sided impact; +, ▽ double-sided impact; ———, NLTV (increasing frequency); ----------, NLTV (decreasing frequency).

where $2b$ is gear backlash. The directional rotation radii λ_p and λ_g for pinion and gear are in the form of

$$\lambda_p = \vec{n}_p \cdot (\vec{j}_p \times \vec{r}_p), \quad \lambda_g = \vec{n}_g \cdot (\vec{r}_g \times \vec{j}_g), \tag{4}$$

where $\vec{r}_p$ and $\vec{r}_g$ are the position vectors of mesh point in the coordinate system S_p and S_g as shown in Fig. 1(b), $\vec{n}_p$ and $\vec{n}_g$ are the unit normal vectors of mesh point, and $\vec{j}_p$ and $\vec{j}_g$ are the unit vectors along pinion and gear rotating axis.

From earlier study, we know that there are two modes expressed in Eq. (1). One is the rigid body rotation and the other is the out-of-phase gear pair torsion that is known as the primary source of excessive gear whine response. Using $p = \delta - e$, Eqs. (1a) and (1b) can be reduced to a single dof equation that only describes the out-of-phase torsion mode as a perturbation about the rigid body motion. Since λ_l changes little with time

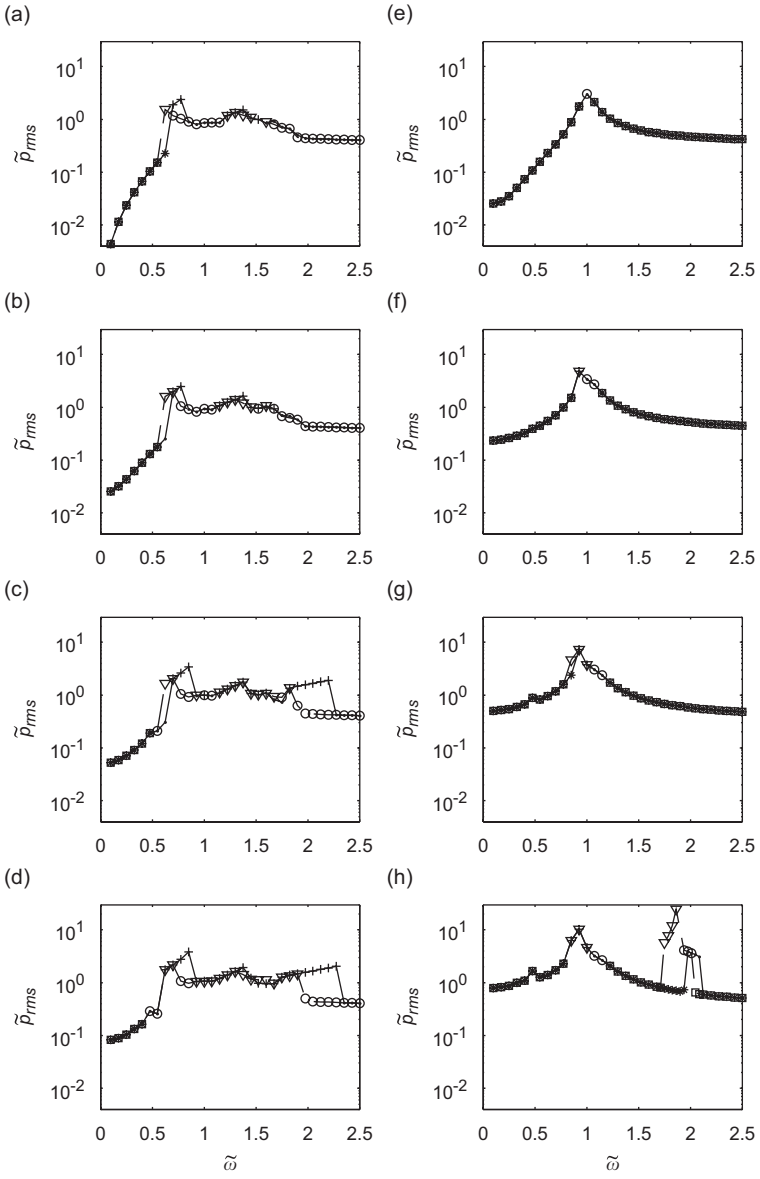

Fig. 6. Effect of mesh stiffness variation on frequency response. Lightly loaded case: $\tilde{T}_p = 0.2$, (a) $\tilde{k}_{a1} = 0$, (b) $\tilde{k}_{a1} = 0.1$, (c) $\tilde{k}_{a1} = 0.2$, (d) $\tilde{k}_{a1} = 0.3$. Heavily loaded case: $\tilde{T}_p = 2$, (e) $\tilde{k}_{a1} = 0$, (f) $\tilde{k}_{a1} = 0.1$, (g) $\tilde{k}_{a1} = 0.2$, (h) $\tilde{k}_{a1} = 0.3$. ∗, □ no impact; ●, ○ single-sided impact; +, ▽ double-sided impact; ———, NLTV (increasing frequency); – – – – – – – – –, NLTV (decreasing frequency).

$\dot{\lambda}_l = \ddot{\lambda}_l = 0$ can be assumed in the derivation in order to obtain the reduced order, definite form equation of motion

$$m_e\ddot{p} + c_m\dot{p} + k_m f(p) = m_e\left(\frac{\lambda_p T_p}{I_p} + \frac{\lambda_g T_g}{I_g} - \ddot{e}\right), \tag{5a}$$

$$m_e = 1/(\lambda_p^2/I_p + \lambda_g^2/I_g), \quad f(p) = \begin{cases} p - b, & p \geqslant b, \\ 0, & -b < p < b, \\ p + b, & p \leqslant -b. \end{cases} \tag{5b}$$

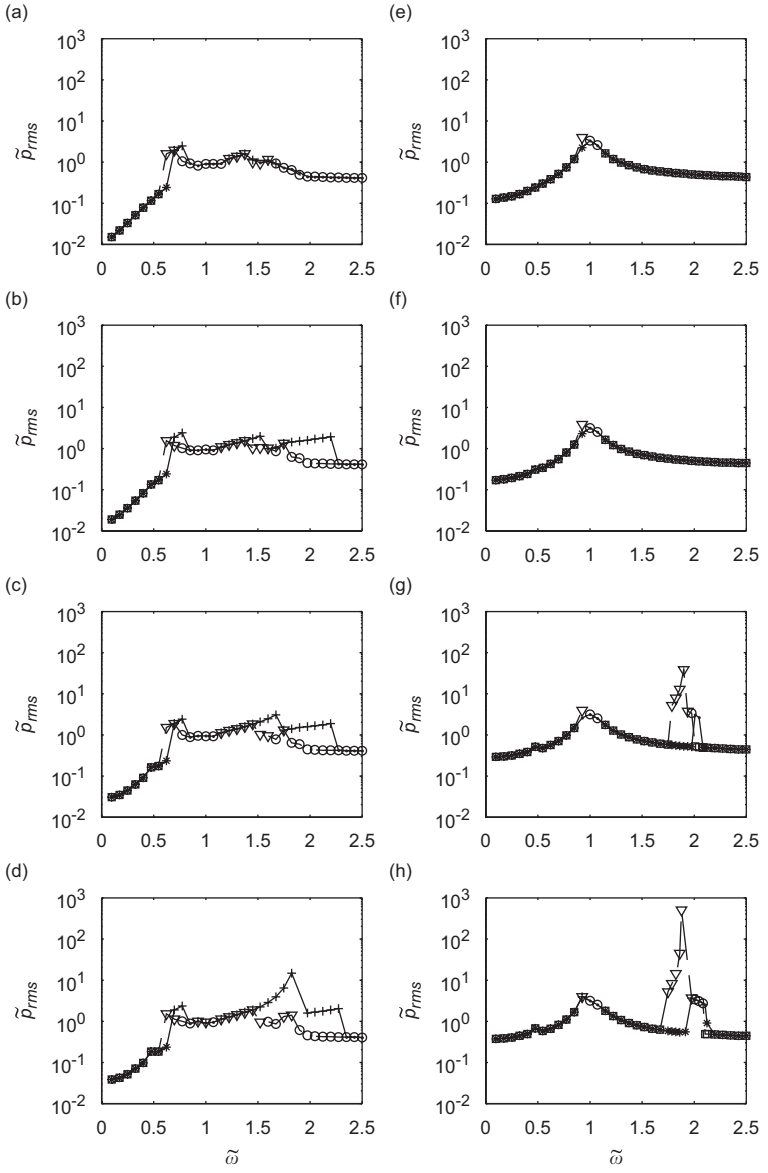

Fig. 7. Effect of directional rotation radius variation on frequency response. Lightly loaded case: $\tilde{T}_p = 0.2$, (a) $\tilde{\lambda}_{pa1} = 0$, (b) $\tilde{\lambda}_{pa1} = 0.1$, (c) $\tilde{\lambda}_{pa1} = 0.15$, (d) $\tilde{\lambda}_{pa1} = 0.18$. Heavily loaded case: $\tilde{T}_p = 2$, (e) $\tilde{\lambda}_{pa1} = 0$, (f) $\tilde{\lambda}_{pa1} = 0.1$, (g) $\tilde{\lambda}_{pa1} = 0.15$, (h) $\tilde{\lambda}_{pa1} = 0.18$. ∗, □ no impact; ●, ○ single-sided impact; +, ▽ double-sided impact; ———, NLTV (increasing frequency); - - - - - - - - -, NLTV (decreasing frequency).

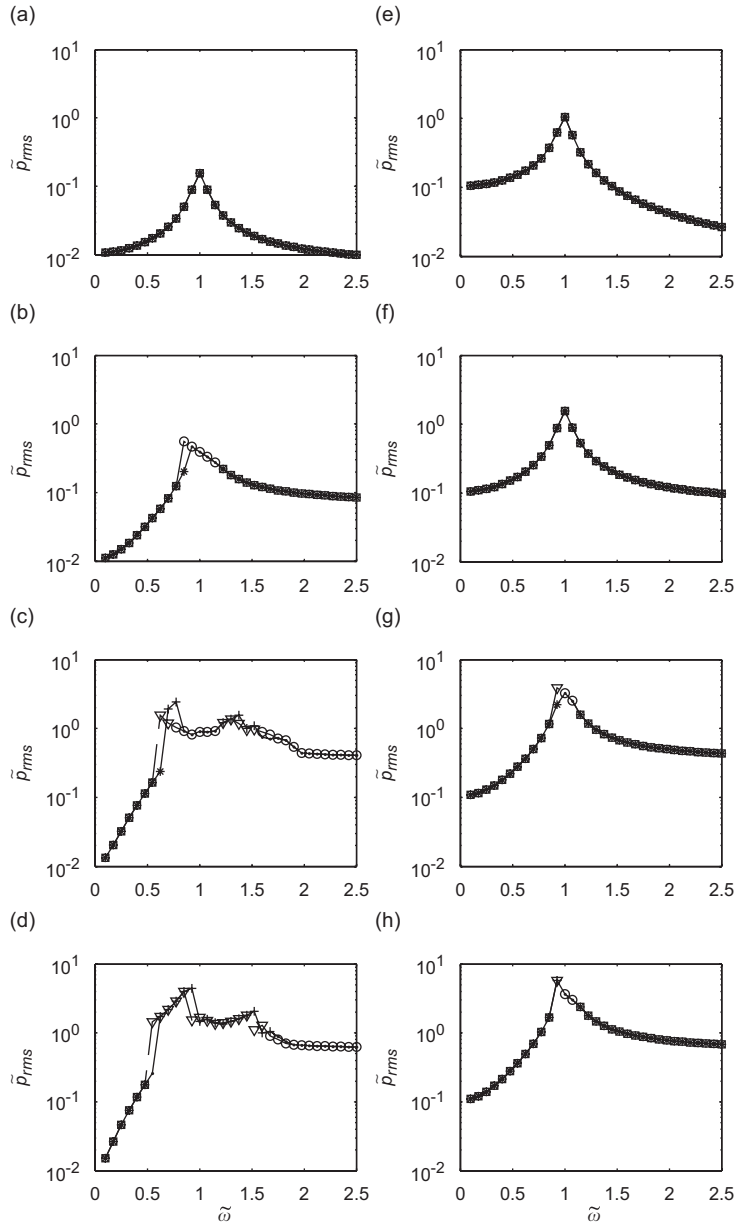

Fig. 8. Effect of kinematic transmission error variation on frequency response. Lightly loaded case: $\tilde{T}_p = 0.2$, (a) $\tilde{e}_{a1} = 0.01$, (b) $\tilde{e}_{a1} = 0.1$, (c) $\tilde{e}_{a1} = 0.5$, (d) $\tilde{e}_{a1} = 0.8$. Heavily loaded case: $\tilde{T}_p = 2$, (e) $\tilde{e}_{a1} = 0.01$, (f) $\tilde{e}_{a1} = 0.1$, (g) $\tilde{e}_{a1} = 0.5$, (h) $\tilde{e}_{a1} = 0.8$. ∗, ○ no impact; ●, ○ single-sided impact; +, ▽ double-sided impact; ————, NLTV (increasing frequency); ----------, NLTV (decreasing frequency).

Next, assuming the following set of dimensionless parameters: $\tilde{p} = p/b$, $\tilde{t} = \omega_n t$, $\tilde{\omega} = \omega/\omega_n$, $\tilde{\lambda}_p = \lambda_p/\lambda_{pm}$, $\tilde{\lambda}_g = \lambda_g/\lambda_{gm}$, $\tilde{k} = k_m/k_{mm}$ and $\tilde{e} = e/b$, a general dimensionless NLTV form of Eq. (5) can be obtained as

$$\tilde{p}'' + 2\xi(\tilde{\lambda}_p^2 + \eta\tilde{\lambda}_g^2)\tilde{p}' + \frac{\tilde{\lambda}_p^2 + \eta\tilde{\lambda}_g^2}{1+\eta}\tilde{k}f(\tilde{p}) = \tilde{T}_p\tilde{\lambda}_p + \tilde{T}_g\tilde{\lambda}_g - \tilde{e}'', \tag{6a}$$

$$\omega_n = \sqrt{k_{mm}/m_{em}}, \tag{6b}$$

$$m_{em} = 1/(\lambda_{pm}^2/I_p + \lambda_{gm}^2/I_g), \tag{6c}$$

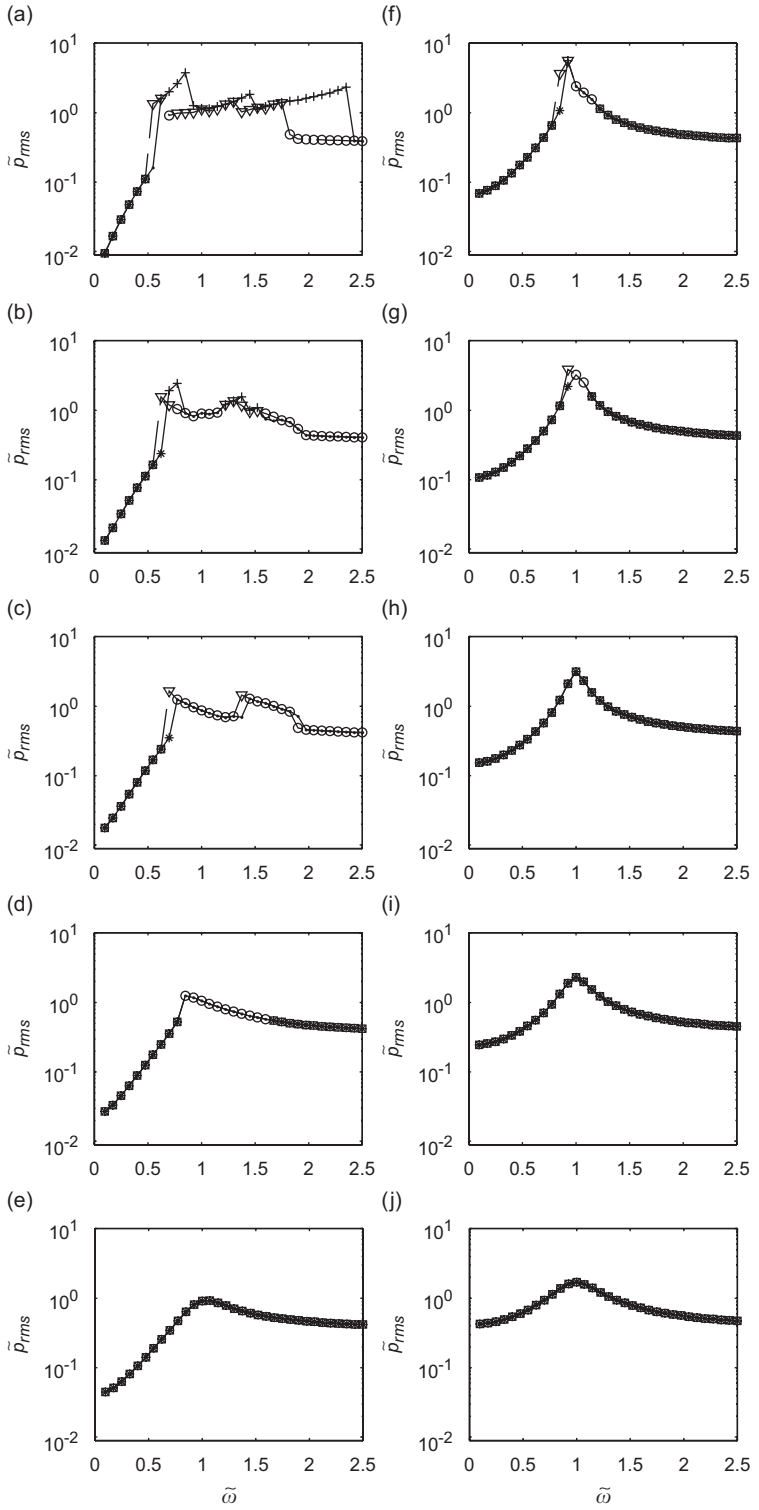

Fig. 9. Effect of system parameter η on frequency response. Lightly loaded case: $\tilde{T}_p = 0.2$, (a) $\eta = 0.1$, (b) $\eta = 0.75$, (c) $\eta = 1.5$, (d) $\eta = 3$, (e) $\eta = 6$. Heavily loaded case: $\tilde{T}_p = 2$, (f) $\eta = 0.1$, (g) $\eta = 0.75$, (h) $\eta = 1.5$, (i) $\eta = 3$, (j) $\eta = 6$. $*$, □ no impact; ●, ○ single-sided impact; $+$, $\bigtriangledown$ double-sided impact; ———, NLTV (increasing frequency); - - - - - - - - -, NLTV (decreasing frequency).

Table 1
Baseline system parameters for a typical automotive hypoid gear pair

Number of pinion teeth	10
Number of gear teeth	43
Pinion offset (m)	0.0318
Gear pitch radius (m)	0.168
Pinion pitch radius (m)	0.048
Mass moment of inertia of pinion ($kg\,m^2$)	0.002
Mass moment of inertia of gear ($kg\,m^2$)	0.05
Backlash (μm)	20
Mesh damping ratio	0.03

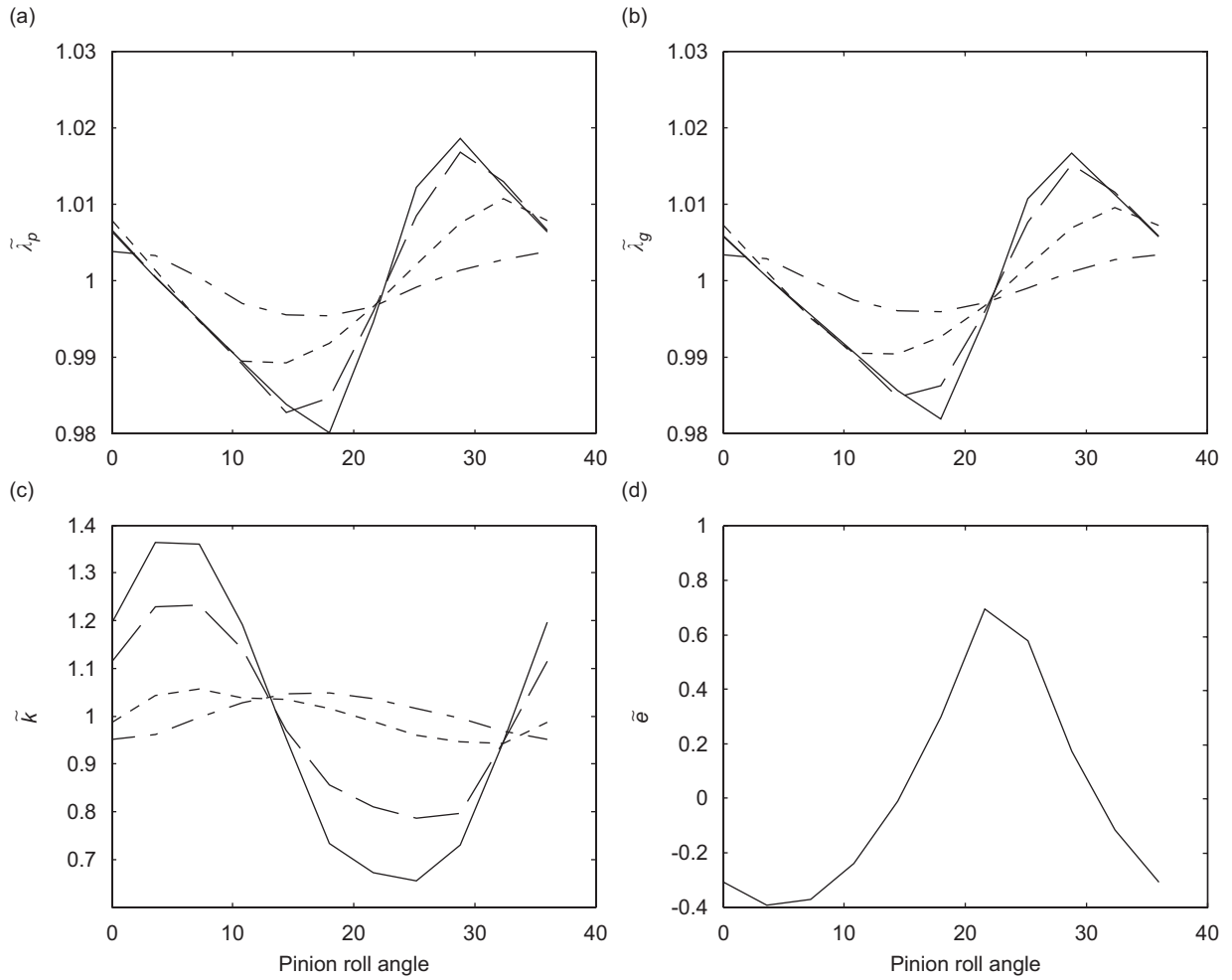

Fig. 10. Computed exact time-varying mesh parameters: (a) Pinion directional rotation radius $\tilde{\lambda}_p$; (b) gear directional rotation radius $\tilde{\lambda}_g$; (c) mesh stiffness $\tilde{k}$; (d) kinematic transmission error $\tilde{e}$. ———, $\tilde{T}_p = 0.65$ (125 N m); ---------, $\tilde{T}_p = 0.98$ (200 N m); · · · · · · · · · · · · , $\tilde{T}_p = 2.01$ (500 N m); - · - · - · - · - · , $\tilde{T}_p = 3.28$ (1000 N m).

$$\xi = \frac{\lambda_{pm}^2 c_m}{2 I_p \omega_n}, \tag{6d}$$

$$\eta = \frac{\lambda_{gm}^2 I_p}{\lambda_{pm}^2 I_g}, \tag{6e}$$

$$\tilde{T}_p = \frac{\lambda_{pm} T_p}{b\omega_n^2 I_p}, \tag{6f}$$

$$\tilde{T}_g = \eta \tilde{T}_p, \tag{6g}$$

where k_{mm} is mean mesh stiffness, and λ_{pm} and λ_{gm} are mean directional rotation radii of pinion and gear, respectively. The dimensionless nonlinear displacement function $f(\tilde{p})$ as shown in Fig. 2 is

$$f(\tilde{p}) = \begin{cases} \tilde{p} - 1, & \tilde{p} \geqslant 1, \\ 0, & -1 < \tilde{p} < 1, \\ \tilde{p} + 1, & \tilde{p} \leqslant -1. \end{cases} \tag{7}$$

If there is no gear backlash, the nonlinear displacement function $f(\tilde{p}) = \tilde{p}$, and Eq. (6a) reduces to a linear time-varying (LTV) form given by

$$\tilde{p}'' + 2\xi(\tilde{\lambda}_p^2 + \eta\tilde{\lambda}_g^2)\tilde{p}' + \frac{\tilde{\lambda}_p^2 + \eta\tilde{\lambda}_g^2}{1+\eta}\tilde{k}\tilde{p} = \tilde{T}_p\tilde{\lambda}_p + \tilde{T}_g\tilde{\lambda}_g - \tilde{e}''. \tag{8}$$

3. Systems with fundamental harmonic

First, we consider only the fundamental harmonic form of the time-varying mesh parameters to study the effects of mesh parameter variations on tooth impact behavior and dynamic response. Dimensionless mesh parameters such as dimensionless directional rotation radii of pinion and gear denoted by $\tilde{\lambda}_p$, $\tilde{\lambda}_g$, mesh stiffness $\tilde{k}$ and kinematic transmission error $\tilde{e}$ could be expressed as the Fourier series

$$\tilde{\lambda}_p = 1 + \sum_{j=1}^{\infty} \tilde{\lambda}_{paj} \cos(j\tilde{\omega}\tilde{t} + \phi_{pj}), \tag{9}$$

$$\tilde{\lambda}_g = 1 + \sum_{j=1}^{\infty} \tilde{\lambda}_{gaj} \cos(j\tilde{\omega}\tilde{t} + \phi_{gj}), \tag{10}$$

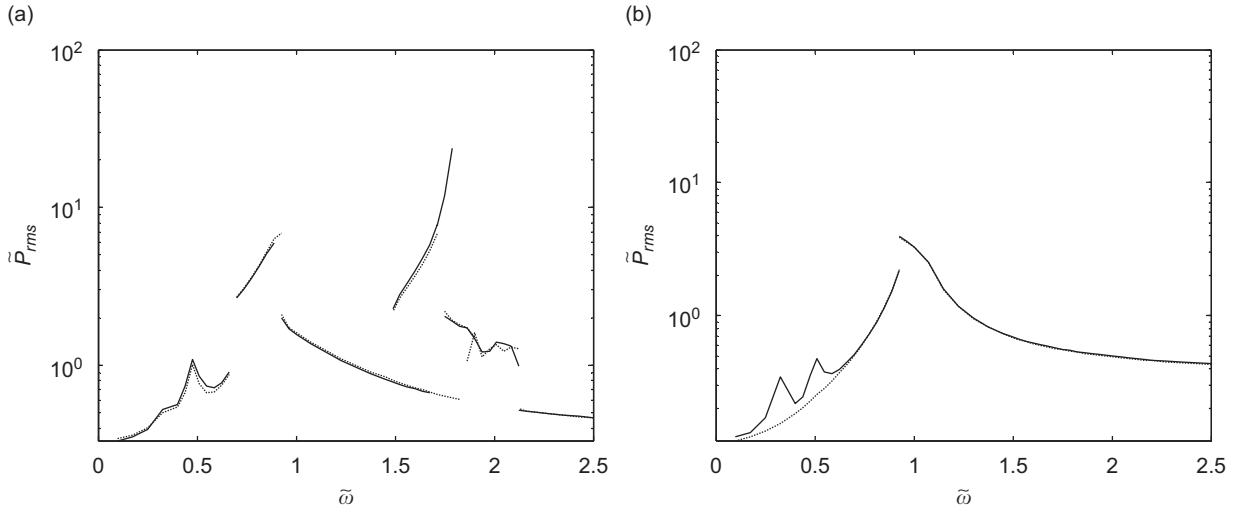

Fig. 11. Frequency response of exact mesh model and fundamental harmonic mesh model: (a) $\tilde{T}_p = 0.65$ (125 N m); (b) $\tilde{T}_p = 2.01$ (500 N m). ———, exact mesh model; · · · · · · · · · · , fundamental harmonic mesh model.

$$\tilde{k} = 1 + \sum_{j=1}^{\infty} \tilde{k}_{aj} \cos(j\tilde{\omega}\tilde{t} + \phi_{kj}), \tag{11}$$

$$\tilde{e} = \sum_{j=1}^{\infty} \tilde{e}_{aj} \cos(j\tilde{\omega}\tilde{t} + \phi_{ej}). \tag{12}$$

In the fundamental harmonic form, they are written as

$$\tilde{\lambda}_p = 1 + \tilde{\lambda}_{pa1} \cos(\tilde{\omega}\tilde{t} + \phi_{p1}), \tag{13}$$

$$\tilde{\lambda}_g = 1 + \tilde{\lambda}_{ga1} \cos(\tilde{\omega}\tilde{t} + \phi_{g1}), \tag{14}$$

$$\tilde{k} = 1 + \tilde{k}_{a1} \cos(\tilde{\omega}\tilde{t} + \phi_{k1}), \tag{15}$$

$$\tilde{e} = \tilde{e}_{a1} \cos(\tilde{\omega}\tilde{t} + \phi_{e1}). \tag{16}$$

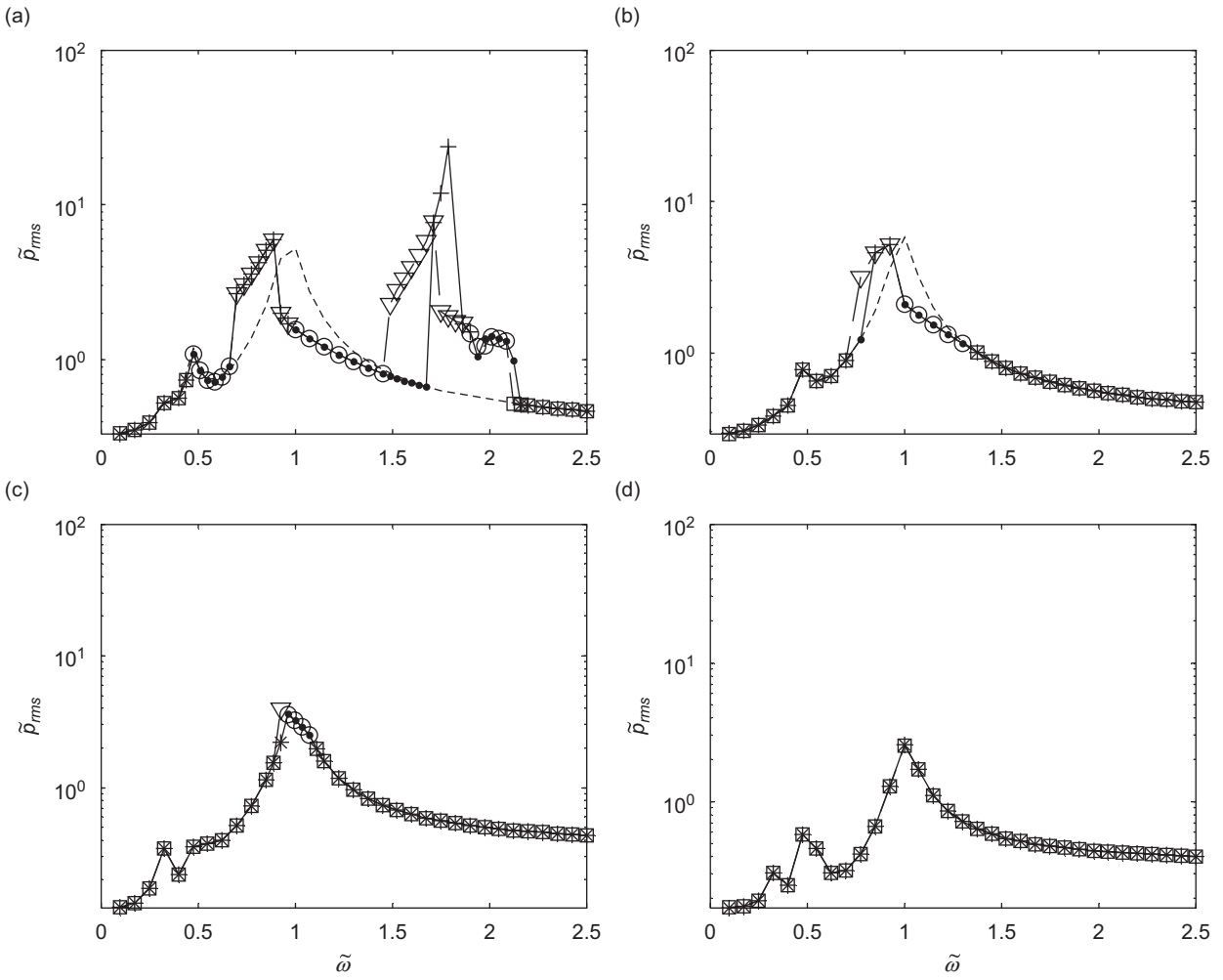

Fig. 12. Effect of mean load on tooth impact: (a) $\tilde{T}_p = 0.65$ (125 N m); (b) $\tilde{T}_p = 0.98$ (200 N m); (c) $\tilde{T}_p = 2.01$ (500 N m); (d) $\tilde{T}_p = 3.28$ (1000 N m). ✻, □ no impact; ●, ○ single-sided impact; +, ▽ double-sided impact; ———, NLTV (increasing frequency); - - - - - - - - -, NLTV (decreasing frequency); · · · · · · · · · · · , LTV.

Substituting Eqs. (13)–(16) into Eq. (6a), a general NLTV equation of motion of a gear pair in the fundamental harmonic form can be obtained as

$$\begin{aligned}&\tilde{p}'' + 2\xi((1+\tilde{\lambda}_{pa1}\cos(\tilde{\omega}\tilde{t}+\phi_{p1}))^2+\eta(1+\tilde{\lambda}_{ga1}\cos(\tilde{\omega}\tilde{t}+\phi_{g1}))^2)\tilde{p}'\\&\quad+\frac{(1+\tilde{\lambda}_{pa1}\cos(\tilde{\omega}\tilde{t}+\phi_{p1}))^2+\eta(1+\tilde{\lambda}_{ga1}\cos(\tilde{\omega}\tilde{t}+\phi_{g1}))^2}{1+\eta}(1+\tilde{k}_{a1}\cos(\tilde{\omega}\tilde{t}+\phi_{k1}))f(\tilde{p})\\&=\tilde{T}_p+\tilde{T}_g+\tilde{T}_p\tilde{\lambda}_{pa1}\cos(\tilde{\omega}\tilde{t}+\phi_{p1})+\tilde{T}_g\tilde{\lambda}_{ga1}\cos(\tilde{\omega}\tilde{t}+\phi_{g1})+\tilde{\omega}^2\tilde{e}_{a1}\cos(\tilde{\omega}\tilde{t}+\phi_{e1}).\end{aligned}\tag{17}$$

Eq. (17) can be partially validated by considering the special case of a spur gear pair. For a spur gear pair, $\tilde{\lambda}_p=\tilde{\lambda}_g=1$, Eq. (17) can be reduced to the equation of motion proposed by Kahraman, which yielded good predictions when compared to the benchmark experimental results [6],

$$\tilde{p}''+2\xi'\tilde{p}'+(1+\tilde{k}_{a1}\cos(\tilde{\omega}\tilde{t}+\phi_{k1}))f(\tilde{p})=\tilde{T}_p+\tilde{T}_g+\tilde{\omega}^2\tilde{e}_{a1}\cos(\tilde{\omega}\tilde{t}+\phi_{e1}),\tag{18}$$

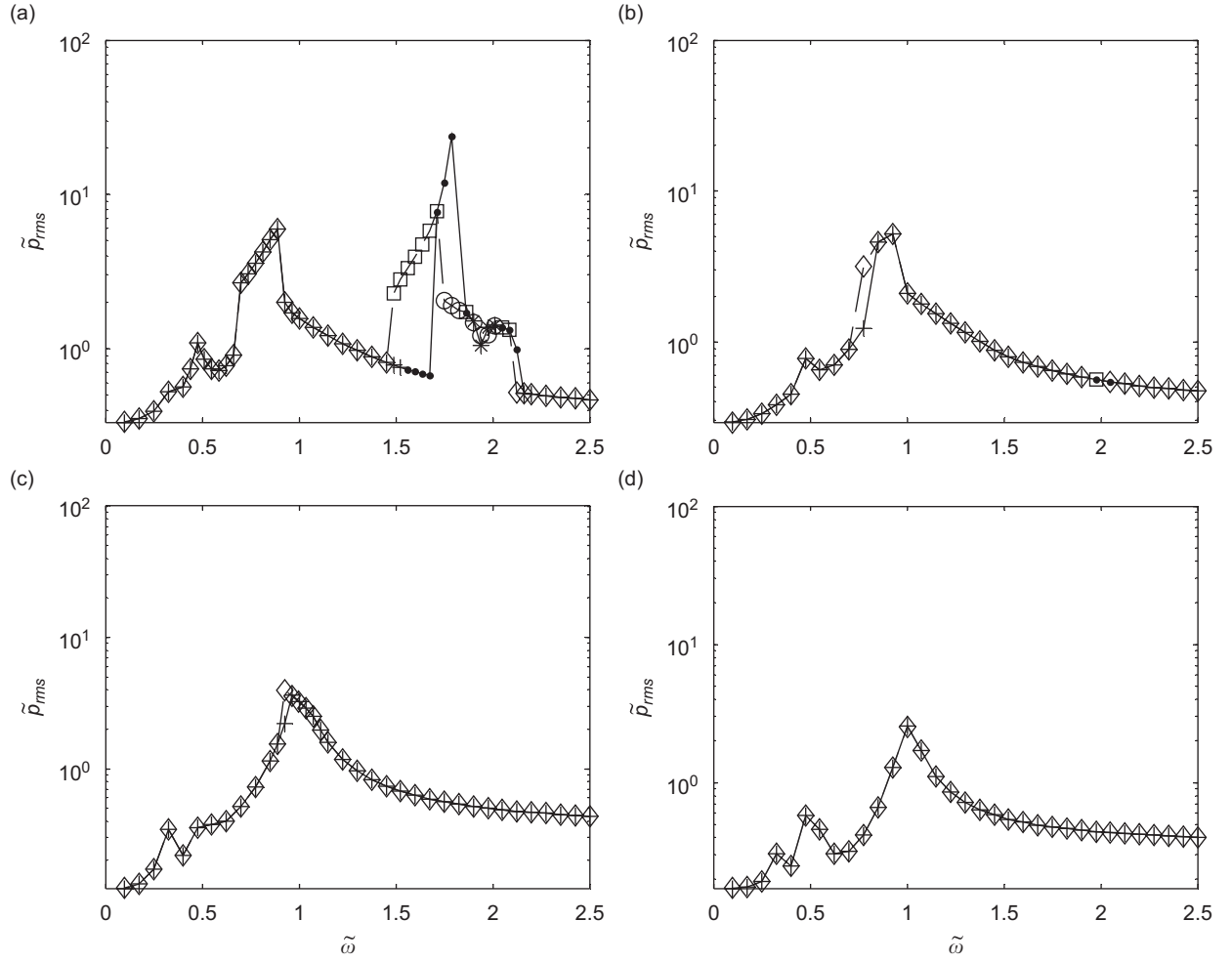

Fig. 13. Effect of mean load on steady-state response: (a) $\tilde{T}_p=0.65$ (125 N m); (b) $\tilde{T}_p=0.98$ (200 N m); (c) $\tilde{T}_p=2.01$ (500 N m); (d) $\tilde{T}_p=3.28$ (1000 N m). +, ◇ period-one response; ●, □ period-n subharmonic response; ∗, ○ quasi-periodic or chaotic response. ———, NLTV (increasing frequency); - - - - - - - - -, NLTV (decreasing frequency).

where $\xi' = \xi(1+\eta)$. Furthermore, the LTV equation of motion in fundamental harmonic form can be expressed as

$$\begin{aligned}\tilde{p}'' &+ 2\xi((1+\tilde{\lambda}_{pa1}\cos(\tilde{\omega}\tilde{t}+\phi_{p1}))^2+\eta(1+\tilde{\lambda}_{ga1}\cos(\tilde{\omega}\tilde{t}+\phi_{g1}))^2)\tilde{p}' \\ &+\frac{(1+\tilde{\lambda}_{pa1}\cos(\tilde{\omega}\tilde{t}+\phi_{p1}))^2+\eta(1+\tilde{\lambda}_{ga1}\cos(\tilde{\omega}\tilde{t}+\phi_{g1}))^2}{1+\eta}(1+\tilde{k}_{a1}\cos(\tilde{\omega}\tilde{t}+\phi_{k1}))\tilde{p} \\ &= \tilde{T}_p+\tilde{T}_g+\tilde{T}_p\tilde{\lambda}_{pa1}\cos(\tilde{\omega}\tilde{t}+\phi_{p1})+\tilde{T}_g\tilde{\lambda}_{ga1}\cos(\tilde{\omega}\tilde{t}+\phi_{g1})+\tilde{\omega}^2\tilde{e}_{a1}\cos(\tilde{\omega}\tilde{t}+\phi_{e1}). \end{aligned} \tag{19}$$

As there is no analytical method exists for the NLTV Eq. (17), the equation is solved by applying the explicit Runge–Kutta integration routine with variable step that is generally applicable to strong nonlinearity. The solution of numerical integration is time domain response $\tilde{p}$, and frequency response can be obtained by root-mean-square (RMS) value $\tilde{p}_{\mathrm{rms}}$ of time domain response (with mean value removed) for each frequency. The algorithm is implemented in MATLAB that is a widely used matrix and numerical analysis program [22].

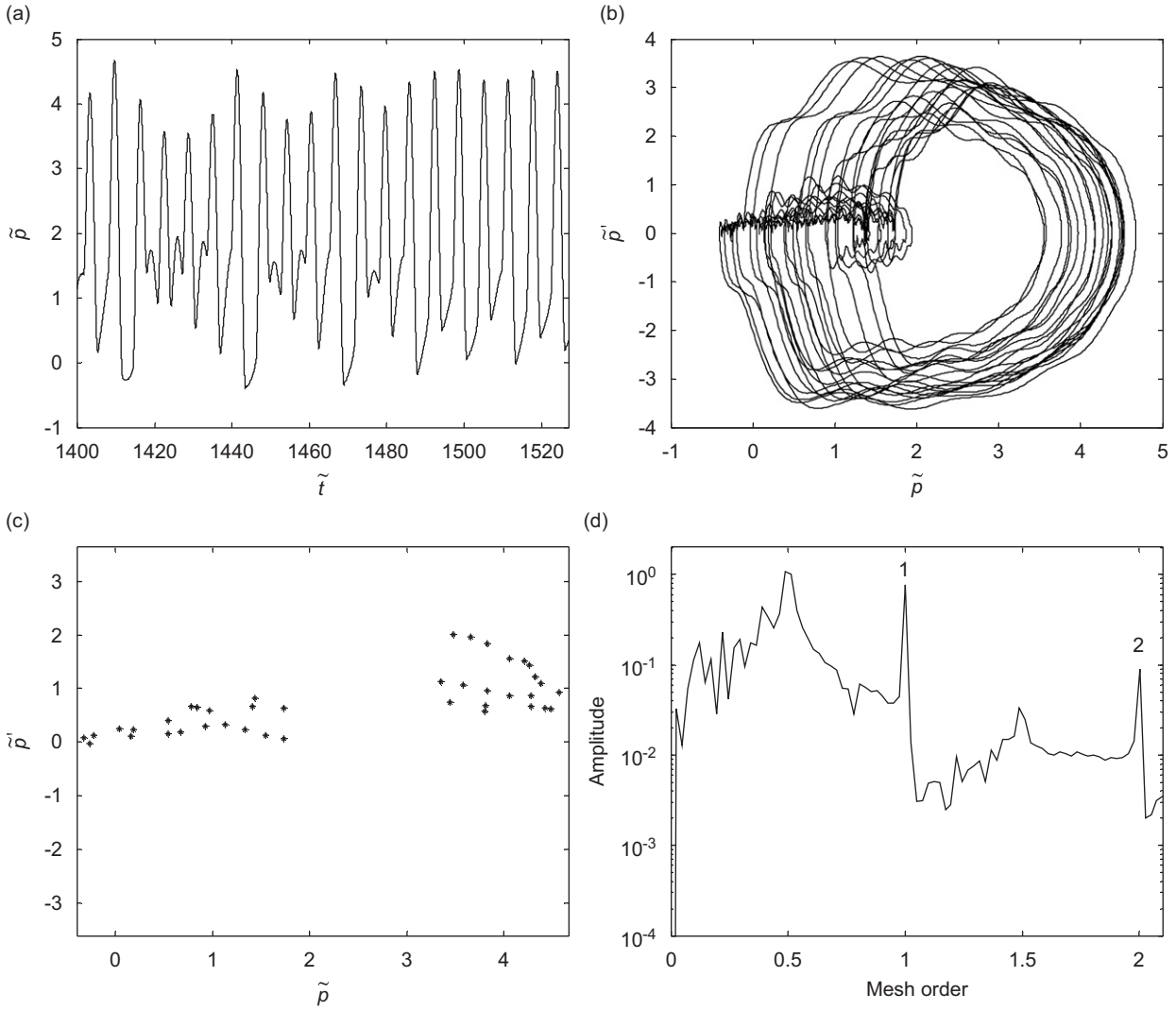

Fig. 14. Chaotic response for $\tilde{T}_p = 0.65$ (125 N m), $\tilde{\omega} = 1.975$: (a) Time history; (b) phase plane; (c) Poincare map; (d) FFT spectrum.

The effects of system parameters such as $\tilde{T}_p$, ξ, $\tilde{k}_{a1}$, $\tilde{\lambda}_{pa1}$, $\tilde{\lambda}_{ga1}$, $\tilde{e}_{a1}$ and η on the frequency response and tooth impact regions are examined next. It may be also noted that tooth impacts may occur due to the gear backlash nonlinearity. There are three possible types of tooth impacts cases: no impact, single-sided impact and double-sided impact, as shown in Fig. 2. Since in most cases $\tilde{\lambda}_{pa1}$ is quite close to $\tilde{\lambda}_{ga1}$, here we assume $\tilde{\lambda}_{pa1} = \tilde{\lambda}_{ga1}$ for simplicity. For our subsequent numerical study, the baseline data used are $\tilde{T}_p = 2$, $\xi = 0.03$, $\tilde{e}_{a1} = 0.5$, $\tilde{k}_{a1} = 0.05$, $\tilde{\lambda}_{pa1} = \tilde{\lambda}_{ga1} = 0.01$, $\eta = 0.75$, $\phi_{p1} = \phi_{g1} = 0$, $\phi_{k1} = -4/5\pi$, $\phi_{e1} = 1/2\pi$.

3.1. Effect of mean load

The effect of mean load on dynamic response is shown in Fig. 3. For lightly loaded case where $\tilde{T}_p = 0.1$, we can see the rich nonlinear behaviors including jump discontinuities coupled with single-sided tooth impacts (denoted by marker ● and ○ for increasing and decreasing frequency, respectively) and double-sided tooth impacts (denoted by marker + and ▽ for increasing and decreasing frequency, respectively) dominating the response. As $\tilde{T}_p$ is increased to 0.2, the jump phenomenon can still be observed but the multivalued transition

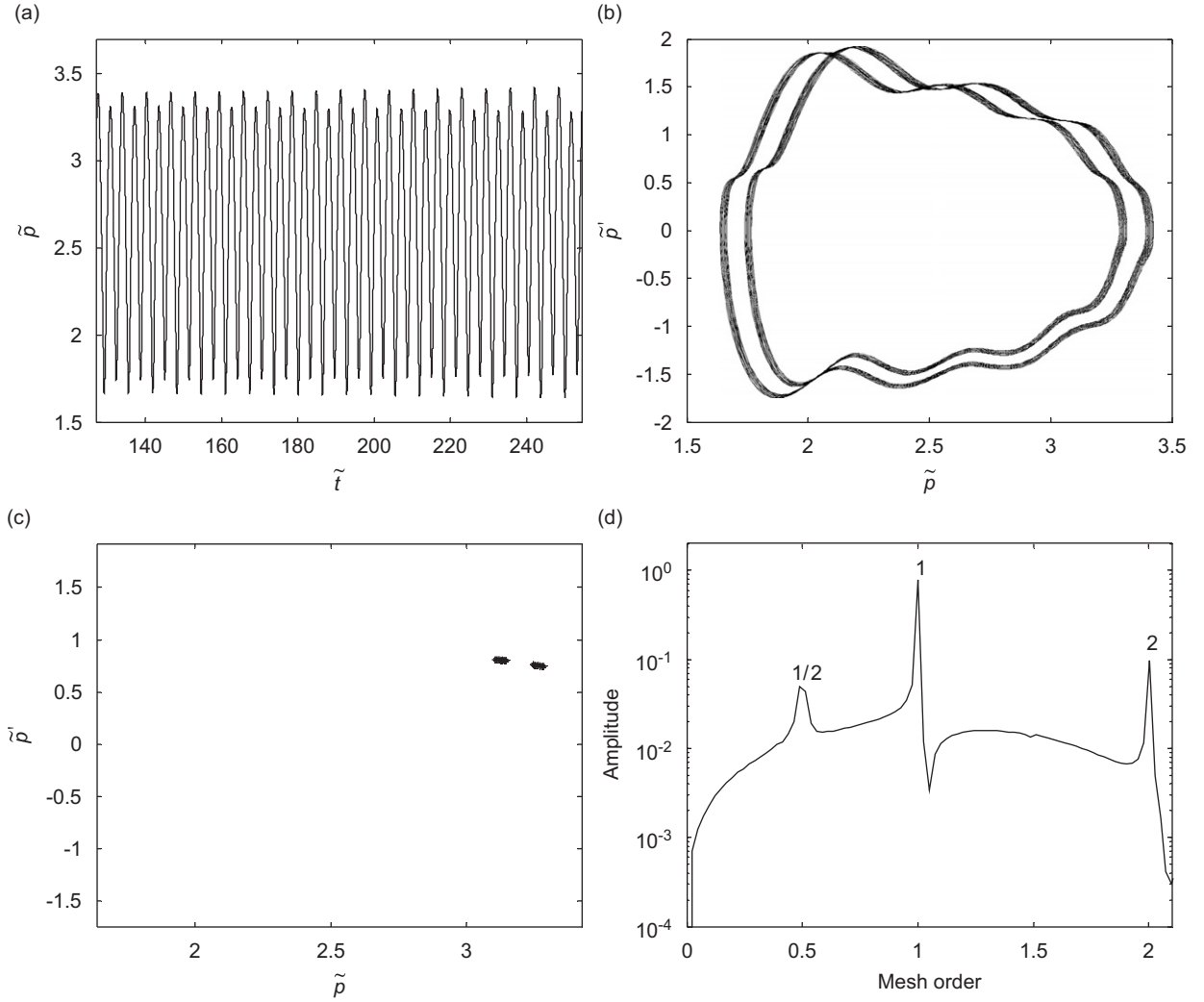

Fig. 15. Subharmonic response for $\tilde{T}_p = 0.98$ (200 N m), $\tilde{\omega} = 1.975$: (a) Time history; (b) phase plane; (c) Poincare map; (d) FFT spectrum.

frequency region between the lower and upper jump discontinuities becomes narrower. Only two jump discontinuities are seen for the case of $\tilde{T}_p = 0.4$ in which one is a softening type and the other is a hardening one. Moreover, wider range of no impacts (denoted by marker ✻ and □ for increasing and decreasing frequency, respectively) appears and the response becomes more predictable. When $\tilde{T}_p$ is increased further to 1.0, there exist only a softening type jump discontinuity and no significant impact behavior is observed. For $\tilde{T}_p = 5$, the mean load becomes large enough to prevent tooth separations, and thus no tooth impacts and jump discontinuities are observed. In this case, the overall frequency response appears linear. Clearly from these results, the increase in mean load tends to decrease the degree of gear backlash nonlinearity.

The various cases of tooth impacts can be observed in the time history plots as shown in Fig. 4. For $\tilde{T}_p = 0.2$ case, there is obviously no tooth impact at $\tilde{\omega} = 0.55$ as shown in Fig. 4(b). As $\tilde{\omega}$ increases to 0.625, the amplitude of the response increases but still there is no tooth impact is observed as shown in Fig. 4(c). At $\tilde{\omega} = 0.7$, the response amplitude increases considerably that causes the sharp jump up in amplitude along with double-sided tooth impact similar to the behavior reported earlier in Jiang's thesis [18]. At $\tilde{\omega} = 0.775$, the amplitude increases further and double-sided tooth impact remains dominant. When $\tilde{\omega}$ increases to 0.85, the amplitude of the response drops causing an abrupt jump down in amplitude as shown in the frequency response. At this frequency point, the response becomes predominantly single-sided tooth impact behavior.

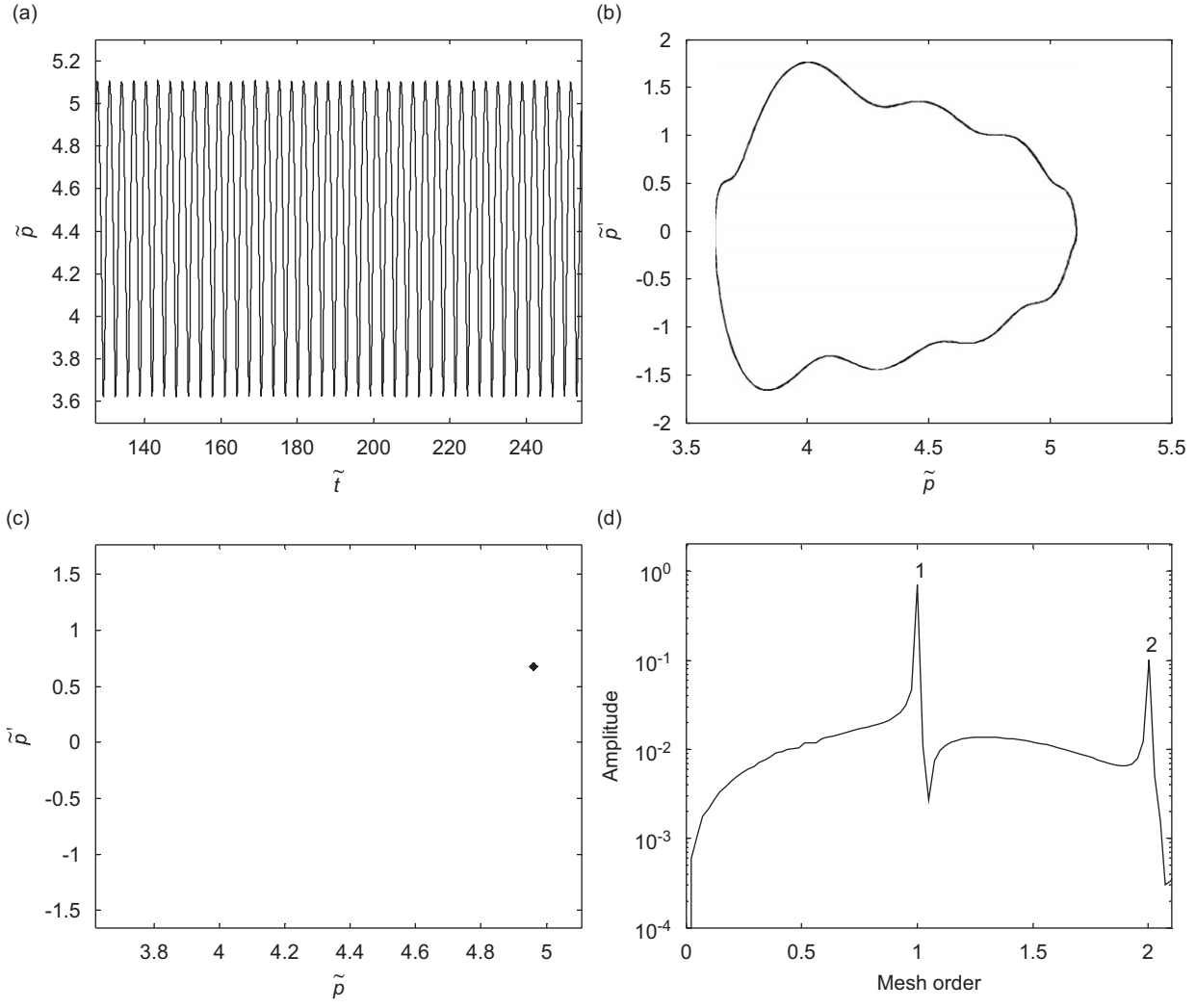

Fig. 16. Period-one response for $\tilde{T}_p = 2.01$ (500 N m), $\tilde{\omega} = 1.975$: (a) Time history; (b) phase plane; (c) Poincare map; (d) FFT spectrum.

3.2. Effect of mesh damping

Mesh damping ratio is another important parameter that affects the frequency response substantially as shown in Fig. 5. As expected, the results show that the frequency response amplitude decreases as ξ is increased for both lightly and heavily loaded cases. For light load case, as ξ is increased, the multivalued frequency region becomes narrower and tooth impacts become alleviated. For heavy load case, ξ affects the jump phenomenon and tooth impact region in a similar way to lightly loaded case but to a lesser extent. There is no tooth impact observed at $\xi = 0.06$, and further increase of ξ will only decrease the response amplitude and make the response behaves more linearly. Hence, the increase in ξ tends to decrease the effect of backlash nonlinearity.

3.3. Effect of mesh stiffness variation

The effect of mesh stiffness variation as the result of the period tooth engagement and disengagement process is examined. As shown in Fig. 6 for light load cases, more jump discontinuities along with single- and double-sided tooth impacts occur as $\tilde{k}_{a1}$ is increased. However, the amplitude of $\tilde{p}_{\mathrm{rms}}$ does not increase by

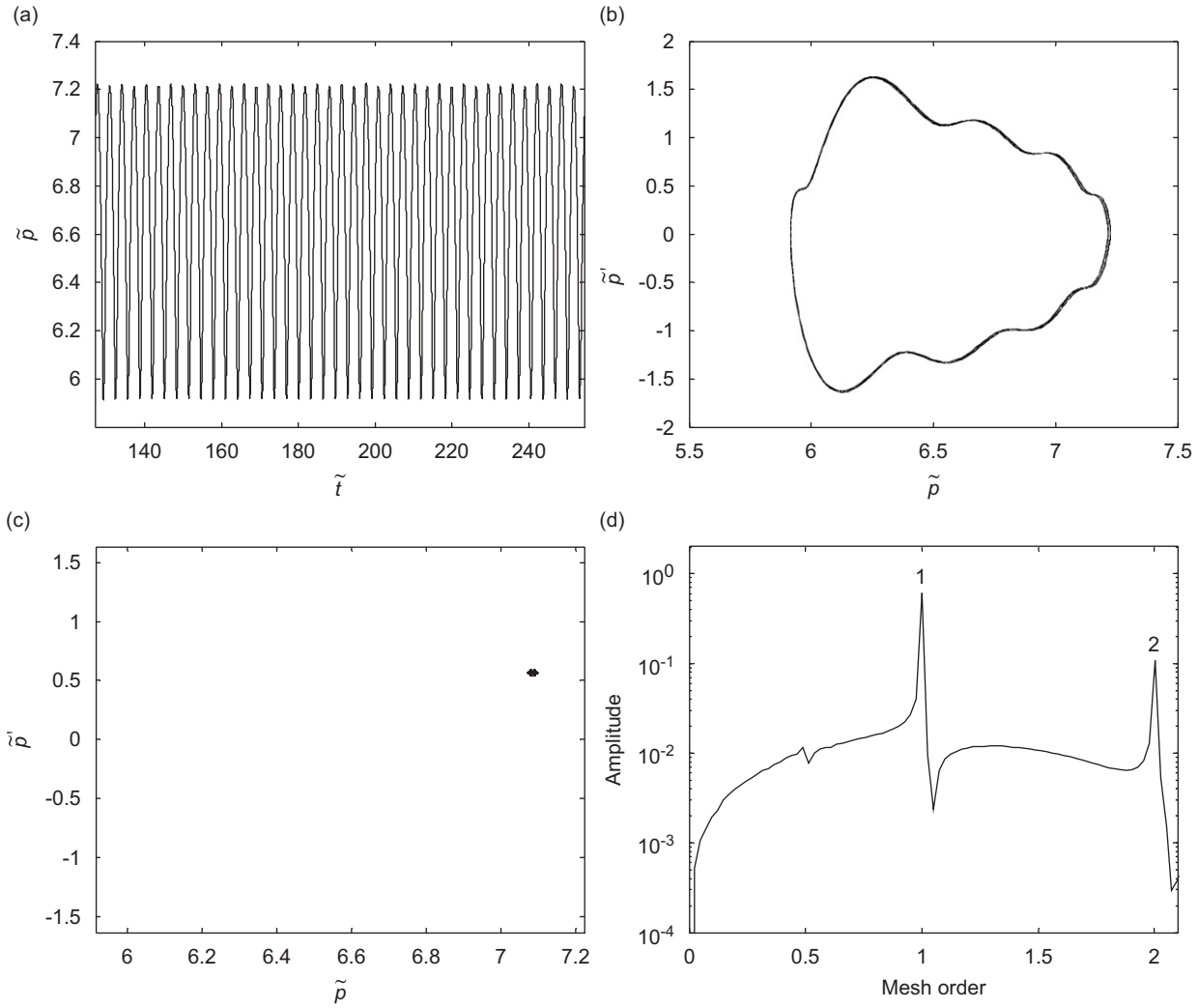

Fig. 17. Period-one response for $\tilde{T}_p = 3.28$ (1000 N m), $\tilde{\omega} = 1.975$: (a) Time history; (b) phase plane; (c) Poincare map; (d) FFT spectrum.

much. A parametric resonance at $\tilde{\omega} = 0.5$ can be clearly observed as $\tilde{k}_{a1}$ is increased to 0.3, which was also identified by Kahraman [6]. For heavily loaded operating conditions, it can be seen that there is no jump discontinuity at $\tilde{k}_{a1} = 0$, only a small jump at $\tilde{k}_{a1} = 0.1$, and very prominent jumps as $\tilde{k}_{a1}$ is increased to 0.3. More single and double-sided tooth impacts appear and the amplitude of $\tilde{p}_{\mathrm{rms}}$ increases with higher value of $\tilde{k}_{a1}$. It indicates that mesh stiffness variation tends to aggravate the effect of backlash nonlinearity, especially for heavily loaded operating condition. This was also found in an earlier study by Kahraman and Singh [6] for spur gears. Furthermore, parametric resonance occurs more readily as $\tilde{k}_{a1}$ is increased to 0.2 and 0.3 as shown in Figs. 6(g) and (h).

3.4. Effect of directional rotation radius variation

The variation in directional rotation radius $\tilde{\lambda}_{pa1}$ is mainly due to the spatial-varying nature of the mesh points. It can be affected by numerous geometrical factors such as tooth errors, gear eccentricity and shaft misalignment. As shown in Fig. 7, for lightly loaded condition, more jump discontinuities along with double-sided tooth impacts occur as $\tilde{\lambda}_{pa1}$ increases, but the amplitude of $\tilde{p}_{\mathrm{rms}}$ does not change considerably. A parametric resonance can be seen to occur at $\tilde{\omega} = 0.5$, as $\tilde{\lambda}_{pa1}$ is increased to 0.18, as shown in Fig. 7(d).

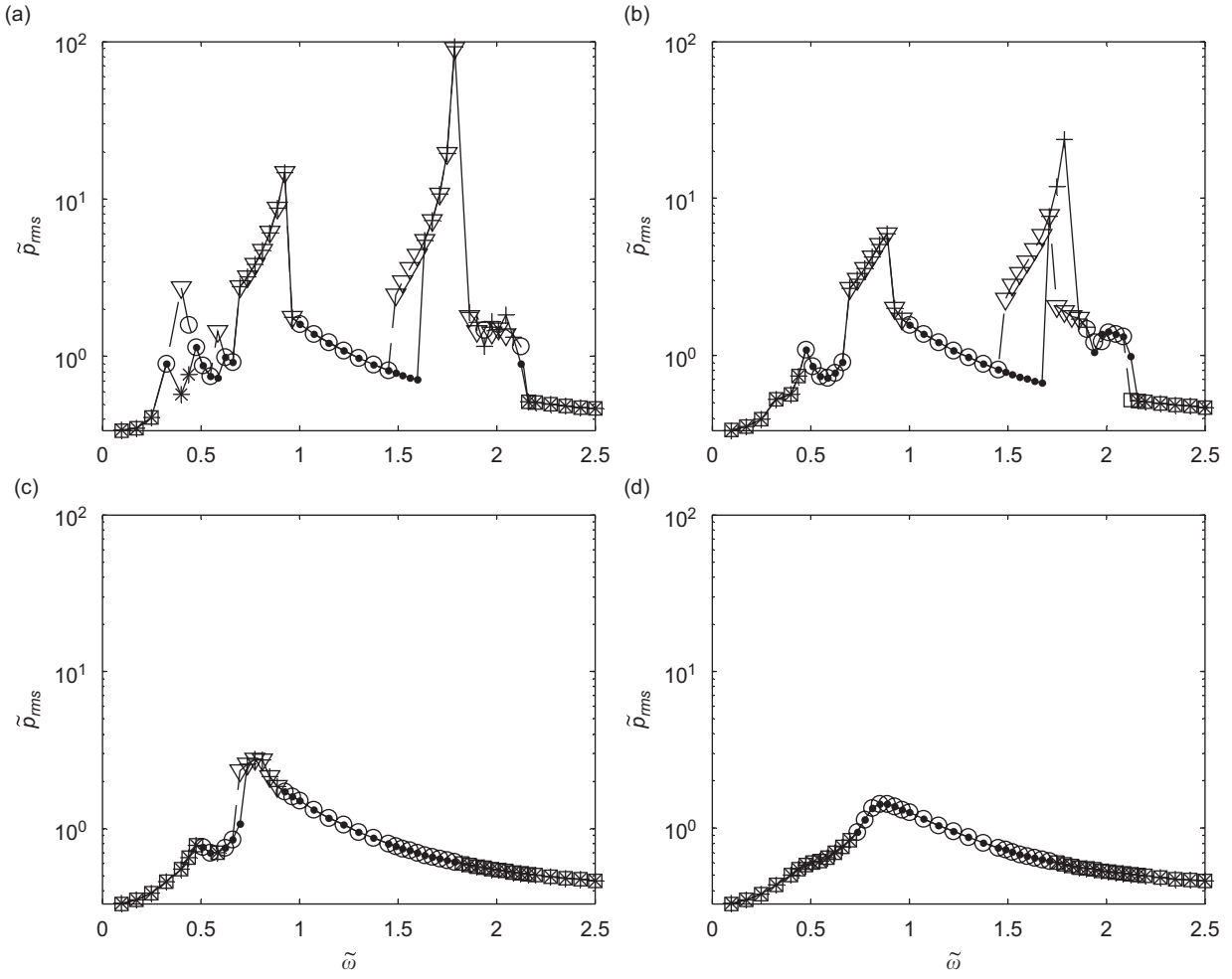

Fig. 18. Effect of mesh damping on tooth impact. $\tilde{T}_p = 0.65$ (125 N m), (a) $\xi = 0.01$; (b) $\xi = 0.03$; (c) $\xi = 0.06$; (d) $\xi = 0.12$. ∗, □ no impact; ●, ○ single-sided impact; +, ▽ double-sided impact; ———, NLTV (increasing frequency); ---------, NLTV (decreasing frequency).

For heavily loaded operating condition, although the response does not change much for $\tilde{\lambda}_{pa1} = 0$ and 0.1, the jump behaviors become more prominent, tooth impacts occur more frequently and the response amplitude increases considerably as $\tilde{\lambda}_{pa1}$ is increased to 0.15 and 0.18. Parametric resonance also occurs as shown in Fig. 7(g) and (h). From these results, it can be concluded that the directional rotation radius variation does aggravate the nonlinearity associated with gear backlash, especially for heavily loaded operation, which is similar to the effect of mesh stiffness variation. However, $\tilde{\lambda}_{pa1}$ is a small value and it is within the range of 0.003–0.02 for most practical hypoid gear sets that we examined. Hence, under normal condition, it is not expected to affect the dynamic response too much. Also, in a normal operating condition, a hypoid gear pair rotates much more smoothly than a spur gear pair even though the line-of-action of the hypoid gear pair changes all the time.

3.5. Effect of kinematic transmission error variation

The kinematic transmission error is a displacement excitation at the mesh point along the line-of-action due to tooth profile deviations. The results are shown in Fig. 8. For lightly loaded case the predicted response shows no jump discontinuity at $\tilde{e}_{a1} = 0.01$, a softening jump when $\tilde{e}_{a1} = 0.1$, both a softening jump and a

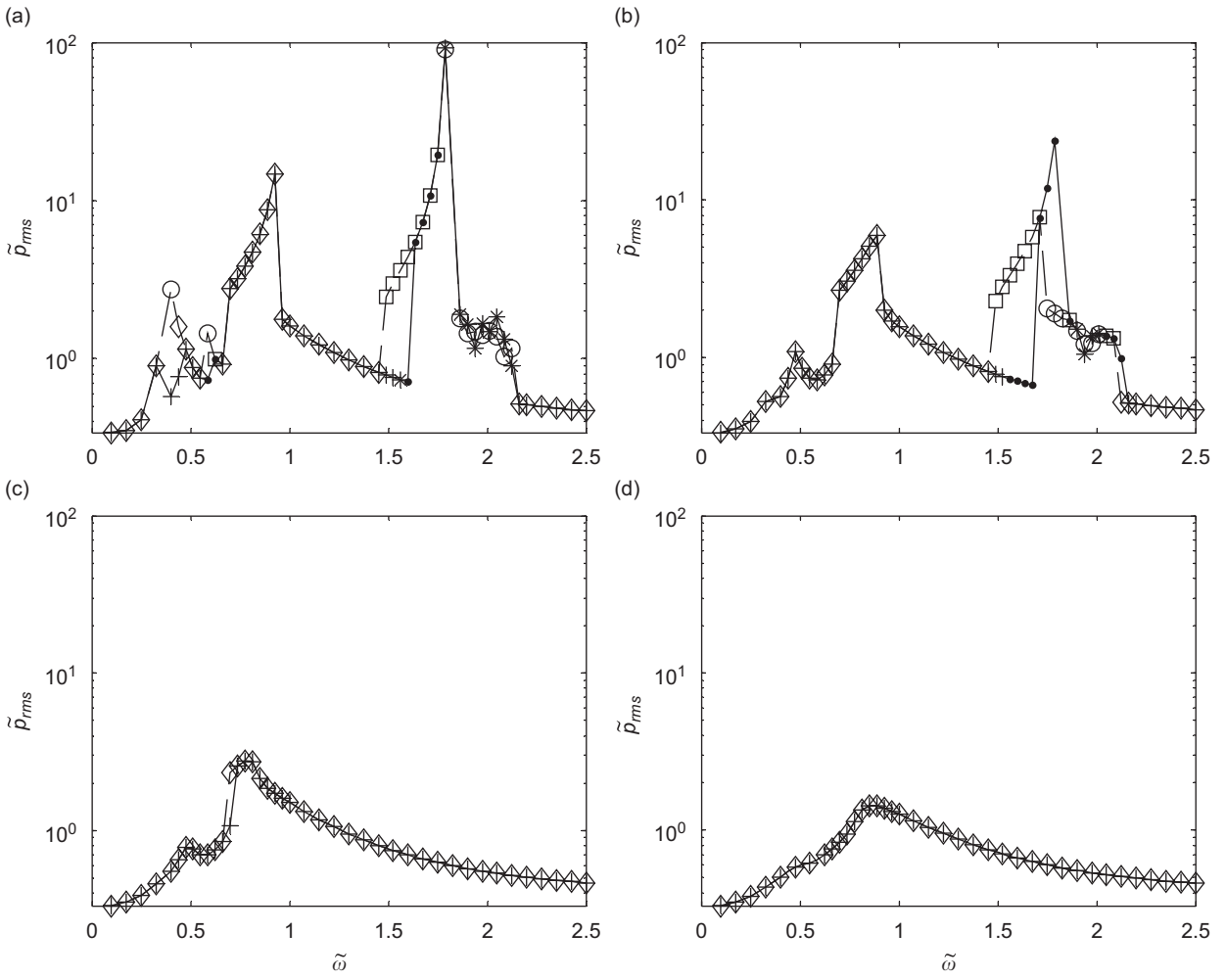

Fig. 19. Effect of mesh damping on steady-state response. $\tilde{T}_p = 0.65$ (125 N m), (a) $\xi = 0.01$; (b) $\xi = 0.03$; (c) $\xi = 0.06$;(d) $\xi = 0.12$. +, ◇ period-one response; ●, □ period-n subharmonic response; ∗, ○ quasi-periodic or chaotic response. ———, NLTV (increasing frequency); ----------, NLTV (decreasing frequency).

hardening jump for $\tilde{e}_{a1} = 0.5$, and very prominent jump behaviors for $\tilde{e}_{a1} = 0.8$. As expected, no tooth impact occurs for $\tilde{e}_{a1} = 0.01$. Single-sided tooth impacts can be seen occurring within a small region around the primary resonance for $\tilde{e}_{a1} = 0.1$. However, when $\tilde{e}_{a1}$ is increased to 0.5 and 0.8, obvious single- and double-sided tooth impacts can be observed. The amplitude of $\tilde{p}_{\mathrm{rms}}$ clearly grows with increasing $\tilde{e}_{a1}$. For heavily loaded operating conditions, $\tilde{e}_{a1}$ can also be seen to affect both jump discontinuity and tooth impact behavior, but to a lesser extent. These results implicate that the kinematic transmission error variation also tends to worsen the degree of backlash nonlinearity, especially for lightly loaded gear pair system.

3.6. *Effect of system parameter η*

System parameter η can be calculated from $\eta = \lambda_{gm}^2 I_p / \lambda_{pm}^2 I_g$ as given in Eq. (6e). As shown in Fig. 9, the response amplitude decreases as η is increased for both lightly and heavily loaded cases. For lightly loaded case, as η is increased, we see less evidence of jump discontinuities along with single and double-sided tooth impacts. At $\eta = 6$, there are no jump discontinuity and tooth impacts at all as shown in Fig. 9(e). For heavily loaded operating condition, η affects the jump phenomenon and tooth impact region in a similar way to lightly

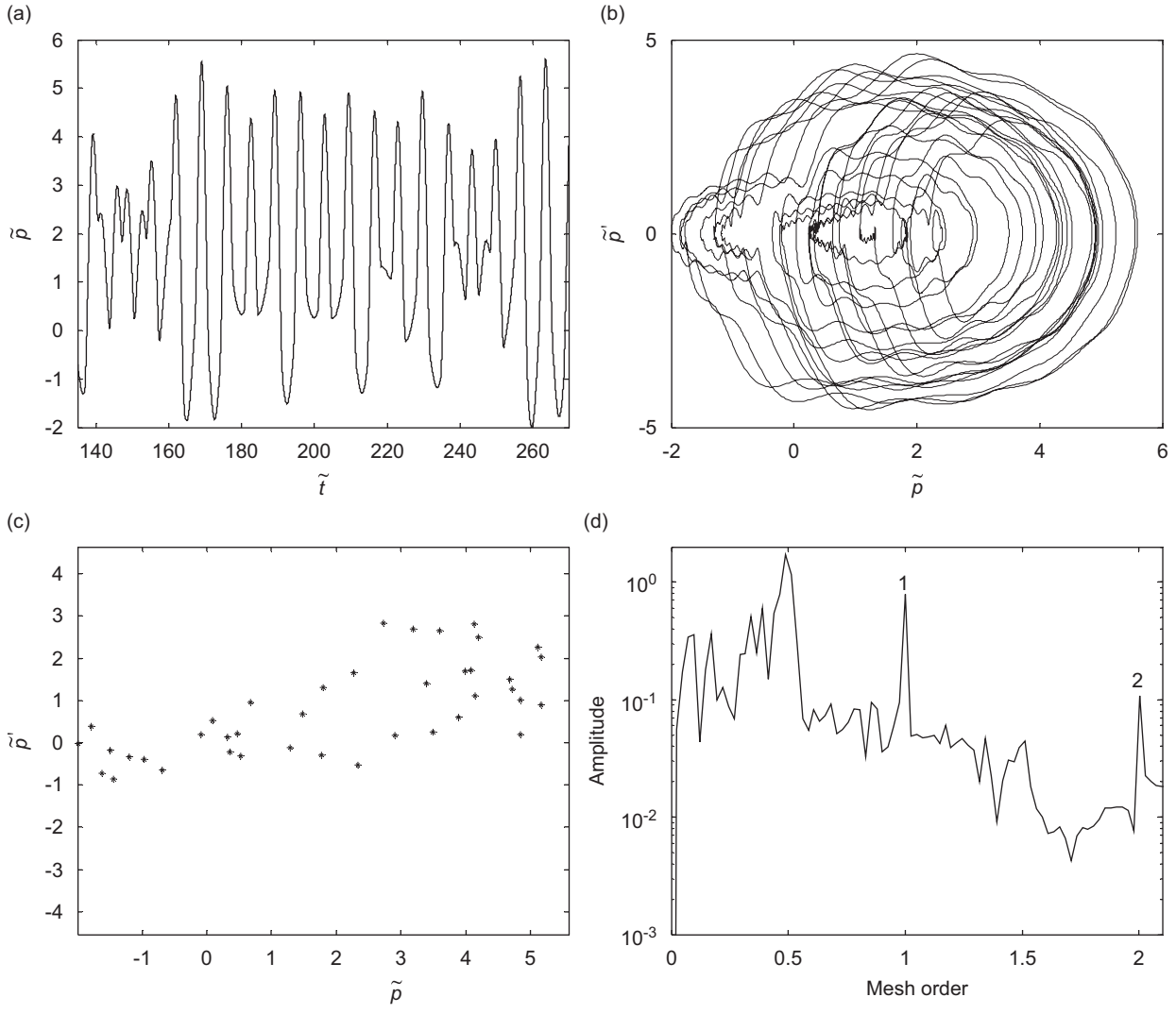

Fig. 20. Chaotic response for $\xi = 0.01$, $\tilde{\omega} = 1.8625$: (a) Time history; (b) phase plane; (c) Poincare map; (d) FFT spectrum.

loaded case but to a lesser extent. At $\eta = 1.5$, there are no jumps nor tooth impacts, and further increase in η will only decrease the response amplitude and cause the response to appear linear. Hence, increasing η decreases the degree of backlash nonlinearity effect especially for light load.

4. Exact time-varying mesh model

A three-dimensional quasi-static-loaded tooth contact analysis is performed by using a highly refined gear contact analysis program [20] to obtain the time-dependent mesh model. By condensing the results of the contact analysis, the mesh parameters including pinion and gear directional rotation radii $\tilde{\lambda}_p$,$\tilde{\lambda}_g$, mesh stiffness $\tilde{k}$, and kinematic transmission error $\tilde{e}$ for each roll angle position are calculated as follows [21]. In contact analysis the contact area is divided into many contact cells. The results of the tooth contact analysis consist of the position vector $\vec{r}_i = (\vec{r}_{ix}, \vec{r}_{iy}, \vec{r}_{iz})$, the normal vector $\vec{n}_i = (\vec{n}_{ix}, \vec{n}_{iy}, \vec{n}_{iz})$, load f_i of each cell i, loaded transmission error e_L and kinematic (unloaded) transmission error e for each roll angle. The total force can be calculated as

$$F_x = \sum_{i=1}^{N} n_{ix} f_i, \tag{20a}$$

$$F_y = \sum_{i=1}^{N} n_{iy} f_i, \tag{20b}$$

$$F_z = \sum_{i=1}^{N} n_{iz} f_i \tag{20c}$$

$$F_{\text{total}} = \sqrt{F_x^2 + F_y^2 + F_z^2}. \tag{20d}$$

Then line-of-action (n_x,n_y,n_z) can be obtained as

$$n_x = F_x/F_{\text{total}}, \tag{21a}$$

$$n_y = F_y/F_{\text{total}}, \tag{21b}$$

$$n_z = F_z/F_{\text{total}}. \tag{21c}$$

The total moment can be derived as

$$M_x = \sum_{i=1}^{N} f_i[n_{iz} r_{iy} - n_{iy} r_{iz}], \tag{22a}$$

$$M_y = \sum_{i=1}^{N} f_i[n_{ix} r_{iz} - n_{iz} r_{ix}], \tag{22b}$$

$$M_z = \sum_{i=1}^{N} f_i[n_{iy} r_{ix} - n_{ix} r_{iy}]. \tag{22c}$$

Finally, the mesh point vector (x, y, z) is derived as

$$y = \frac{\sum_{i=1}^{N} r_{iy} fi}{\sum_{i=1}^{N} f_i}, \tag{23a}$$

$$x = (M_z + F_x y)/F_y, \tag{23b}$$

$$z = (M_y + F_z x)/F_x. \tag{23c}$$

Here, the mesh stiffness is defined as

$$k_m = F_{\text{total}}/(e_L - e), \tag{24}$$

where e_L and e are loaded and kinematic (unloaded) transmission error along line-of-action direction.

The directional rotation radii λ_p and λ_g can be calculated by Eq. (4), and the dimensionless mesh parameters can be calculated from

$$\tilde{\lambda}_p = \lambda_p/\lambda_{pm}, \tag{25}$$

$$\tilde{\lambda}_g = \lambda_g/\lambda_{gm}, \tag{26}$$

$$\tilde{k} = k_m/k_{mm}, \tag{27}$$

$$\tilde{e} = e/b. \tag{28}$$

Unlike the harmonic form mentioned previously, the condensed mesh parameters $\tilde{\lambda}_p$, $\tilde{\lambda}_g$, $\tilde{k}$ and $\tilde{e}$ are applied in an exact form using a fine interpolation scheme and fed into the subsequent dynamic model represented by Eq. (6a). The explicit Runge–Kutta integration routine with variable step, which is applicable to strong nonlinearity is applied in our analysis to solve the nonlinear ordinary differential equation (6a). Frequency response is obtained by the RMS value of time domain response for each frequency. The algorithm is also implemented in MATLAB [22]. Since the exact time-varying mesh model describes the true, instantaneous gear mesh characteristics, it is expected to predict the gear dynamic response more accurately.

A typical automotive hypoid gear pair is analyzed next to determine the capability of the proposed model. Using the formulation provided above, the system parameters are shown in Table 1. The mesh parameters for various levels of mean loads are calculated for each pinion roll angle position within one mesh cycle as shown in Fig. 10. As expected the peak-to-peak values of $\tilde{\lambda}_p$,$\tilde{\lambda}_g$ and $\tilde{k}$ decreases as mean load is increased, while the kinematic transmission error $\tilde{e}$ does not change at all. Then, $\tilde{\lambda}_p$, $\tilde{\lambda}_g$, $\tilde{k}$ and $\tilde{e}$ are inserted into the NLTV Eq. (6a) for dynamic calculation.

The frequency response results of the exact time-varying mesh model and the fundamental harmonic mesh model discussed previously are compared next. Then the effects of mean load and mesh damping are studied since it is common knowledge that these two terms are important parameters affecting tooth impacts and steady-state response.

4.1. Comparison of results of exact time-varying and fundamental harmonic mesh models

The frequency response results derived from the exact time-varying mesh model and the formulation in fundamental harmonic form are compared in Fig. 11. For light load $\tilde{T}_p = 0.65$, although the response of the fundamental harmonic mesh model matches well with the exact time-varying mesh model at certain frequencies especially when linear behavior exists, some discrepancies can be seen at frequencies containing nonlinear response away from the fundamental mesh mode. For heavy load $\tilde{T}_p = 2.01$, the fundamental harmonic mesh response shows good agreement with the exact time-varying mesh response in most frequency range except at low frequencies where off-resonance harmonics occur, which is not captured by the simpler fundamental harmonic mesh form. These limited results basically indicate that the proposed exact time-varying mesh model is able to predict the response governed by the fundamental mesh harmonic as well as capture the additional nonlinear response due to the higher harmonics not represented in the simpler fundamental mesh harmonic model. The differences between these two models are more acute in lightly loaded condition since nonlinear response is more predominant in this case compared to the heavier load case.

4.2. Effect of mean load on tooth impact and steady-state response

4.2.1. Effect of mean load on tooth impact

The frequency response of the geared system of interest is computed for a set of mean loads ranging from 125 to 1000 N m. The results are given in Fig. 12. For the case of $\tilde{T}_p = 0.65$, several jump discontinuities can be observed and the response is dominated by single and double-sided impacts. As $\tilde{T}_p$ is increased to 0.98, there are only one softening jump and one hardening jump, and the tooth impacts occur primarily in a narrower region of $0.775 < \tilde{\omega} < 1.3$. For $\tilde{T}_p = 2.01$, only a softening jump and a small region of tooth impacts occur near the primary resonance. When $\tilde{T}_p$ is increased to 3.28, there are no visible jump discontinuities and tooth impacts at all. In this high mean load case, the dynamic response appears to behave quite linearly. Also, as $\tilde{T}_p$ is increased, the dynamic response amplitude decreased.

The above observation can be explained as follows. As seen in the earlier analysis, when mean load increases, the degree of variations in the pinion and gear directional rotation radius and mesh stiffness decrease. These smaller variations along with higher mean load reduce the degree of nonlinearity due to backlash in the gear pair. Therefore, high mean load generally yields a more linear system response.

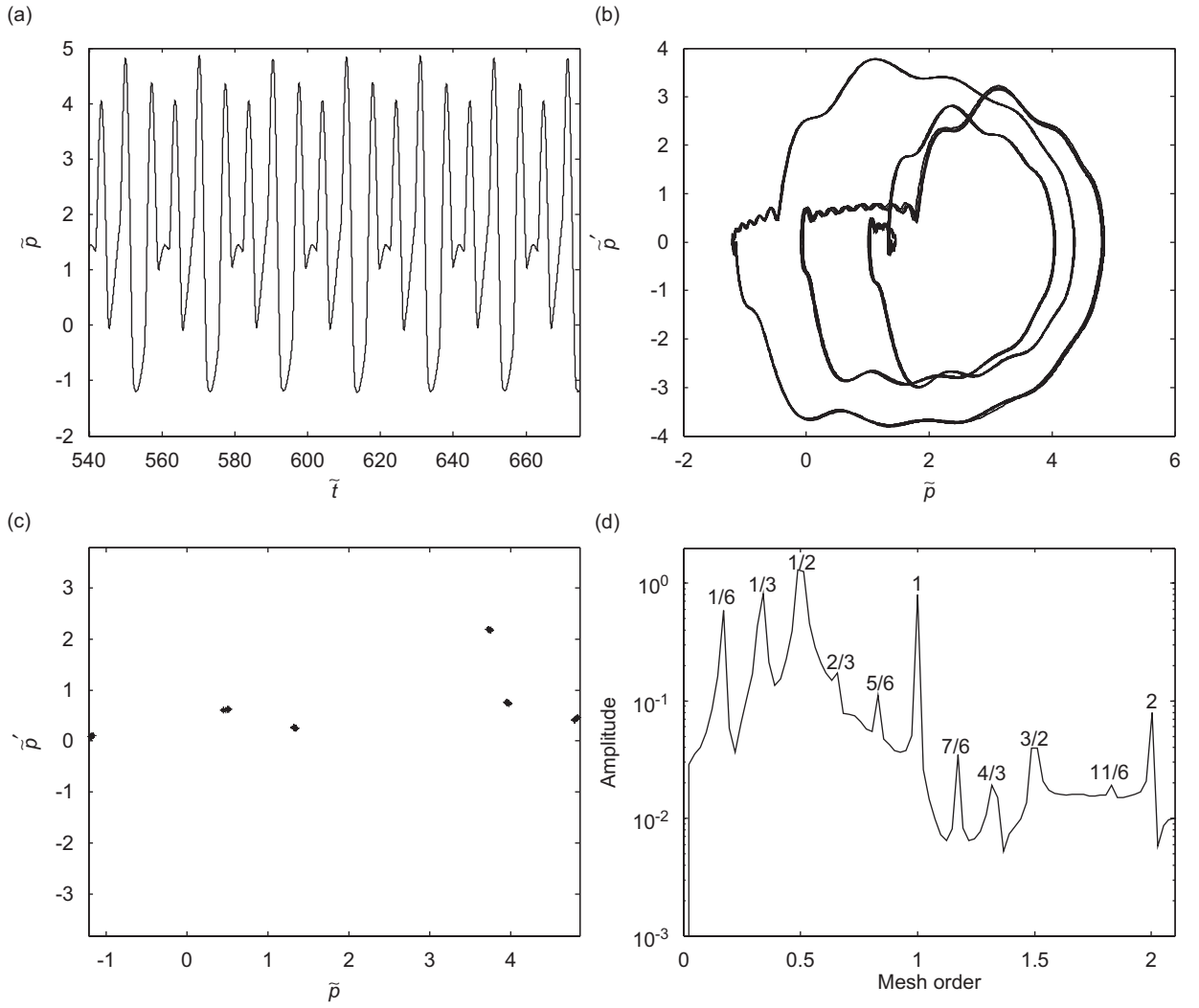

Fig. 21. Subharmonic response for $\xi = 0.03$, $\tilde{\omega} = 1.8625$: (a) time history; (b) phase plane; (c) Poincare map; (d) FFT spectrum.

4.2.2. Effect of mean load on steady-state response

The results of the effect of mean load are re-plotted in Fig. 13 to highlight its influence on steady-state response. As observed in Fig. 13 for $\tilde{T}_p = 0.65$ case (light load condition), a substantial region of subharmonic, quasi-periodic or chaotic response is seen. As $\tilde{T}_p$ is increased to 0.98, the sub-harmonic response begin to weaken and can only be found around $\tilde{\omega} = 1.975$. For $\tilde{T}_p = 2.01$ and 3.28 cases, the frequency response becomes completely period-one. Further clarity on the effect of mean load on frequency response can be obtained by examining the predicted data in other forms as discussed next.

The time history function, phase plane plot, Poincare map and fast Fourier transform (FFT) spectrum plots of the steady-state responses at $\tilde{\omega} = 1.975$ for numerous mean loads are compared in Figs. 14–17. Fig. 14 shows chaotic response for the case of $\tilde{T}_p = 0.65$. Here, the time history is non-periodic (period $\to \infty$), Poincare map contains as many discrete points as the number of periods used in the dynamic analysis, and FFT spectrum depicts broad band characteristic. For $\tilde{T}_p$ equals 0.98, a period-two subharmonic response can be seen at $\tilde{\omega} = 1.975$, as shown in Fig. 15. The time history possesses a period equal to $2T$ ($T = 2\pi/\tilde{\omega}$), Poincare map has two discrete points, and FFT spectrum contains a peak at mesh order $\frac{1}{2}$ in addition to response peaks at orders 1 and 2. Figs. 16 and 17 for $\tilde{T}_p = 2.01$ and 3.28 show period-one responses where

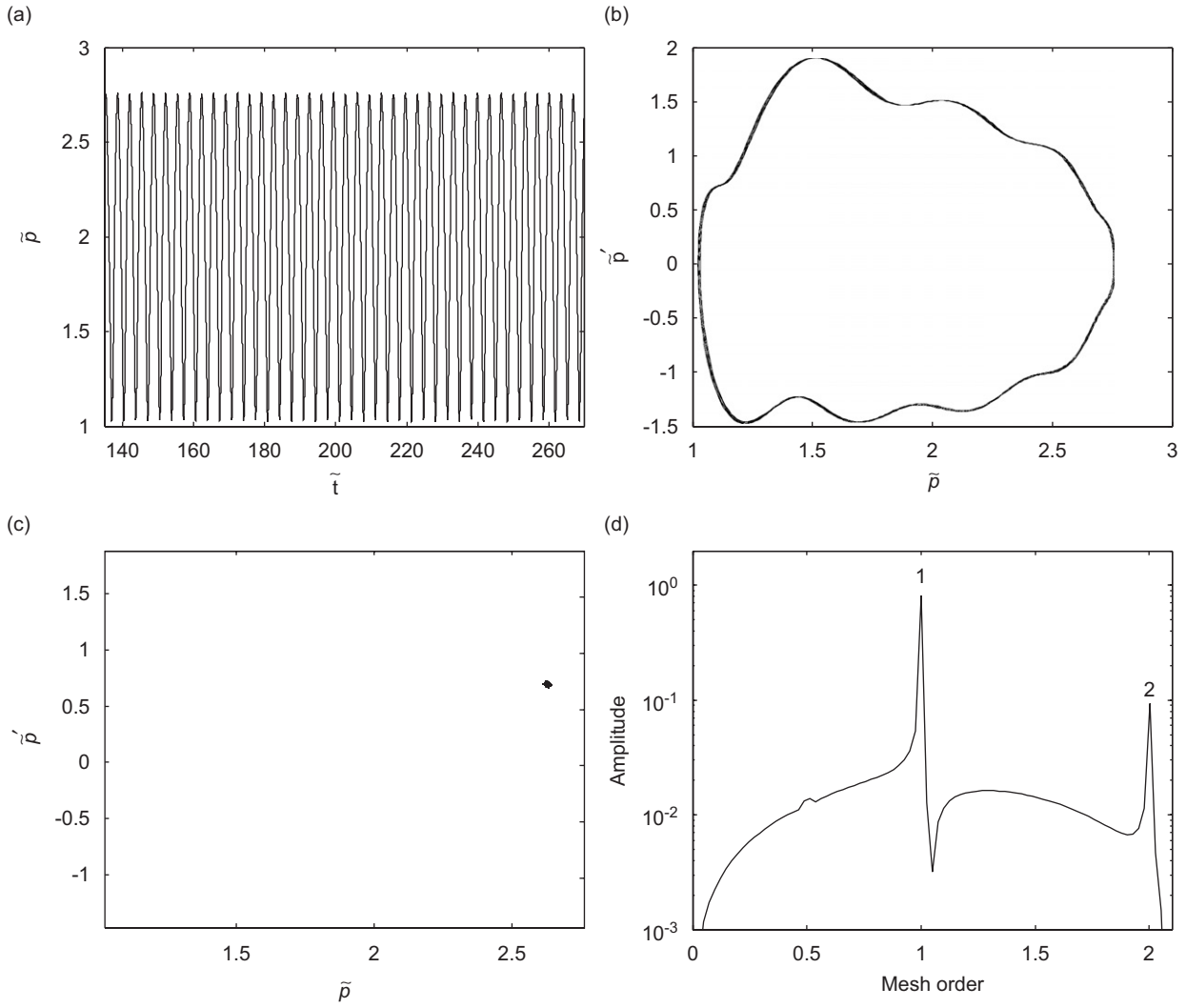

Fig. 22. Period-one response for $\xi = 0.06$, $\tilde{\omega} = 1.8625$: (a) time history; (b) phase plane; (c) Poincare map; (d) FFT spectrum.

their time history functions have a period T, Poincare map shows one discrete points, and FFT spectrum contains only peaks only at mesh orders 1 and 2. These results show that when mean load is progressively increased, the initial chaotic response at $\tilde{\omega} = 1.975$ becomes period-two sub-harmonic response, and subsequently period-one response.

4.3. Effect of mesh damping on tooth impact and steady-state response

4.3.1. Effect of mesh damping on tooth impact

Next, the effect of mesh damping on tooth impact behavior and steady-state response is investigated using the results shown in Figs. 18 and 19. For light damping $\xi = 0.01$, several jump discontinuities can be seen to occur, and both single- and double-sided impacts dominate the response. As ξ is increased to 0.03, the extent and severity of jumps and tooth impacts reduce. For $\xi = 0.06$ case, only a small number of jumps can be observed and tooth impacts disappear further in the off-resonance region. When ξ is increased to 0.12, there are no observable jumps and only a narrow region around the primary gear pair torsional resonance is dictated by single-sided impacts. The response amplitude also decreases considerably as ξ is increased, as expected. From these plots, we can conclude that the increase in ξ will cause the dynamic response to behave more linearly.

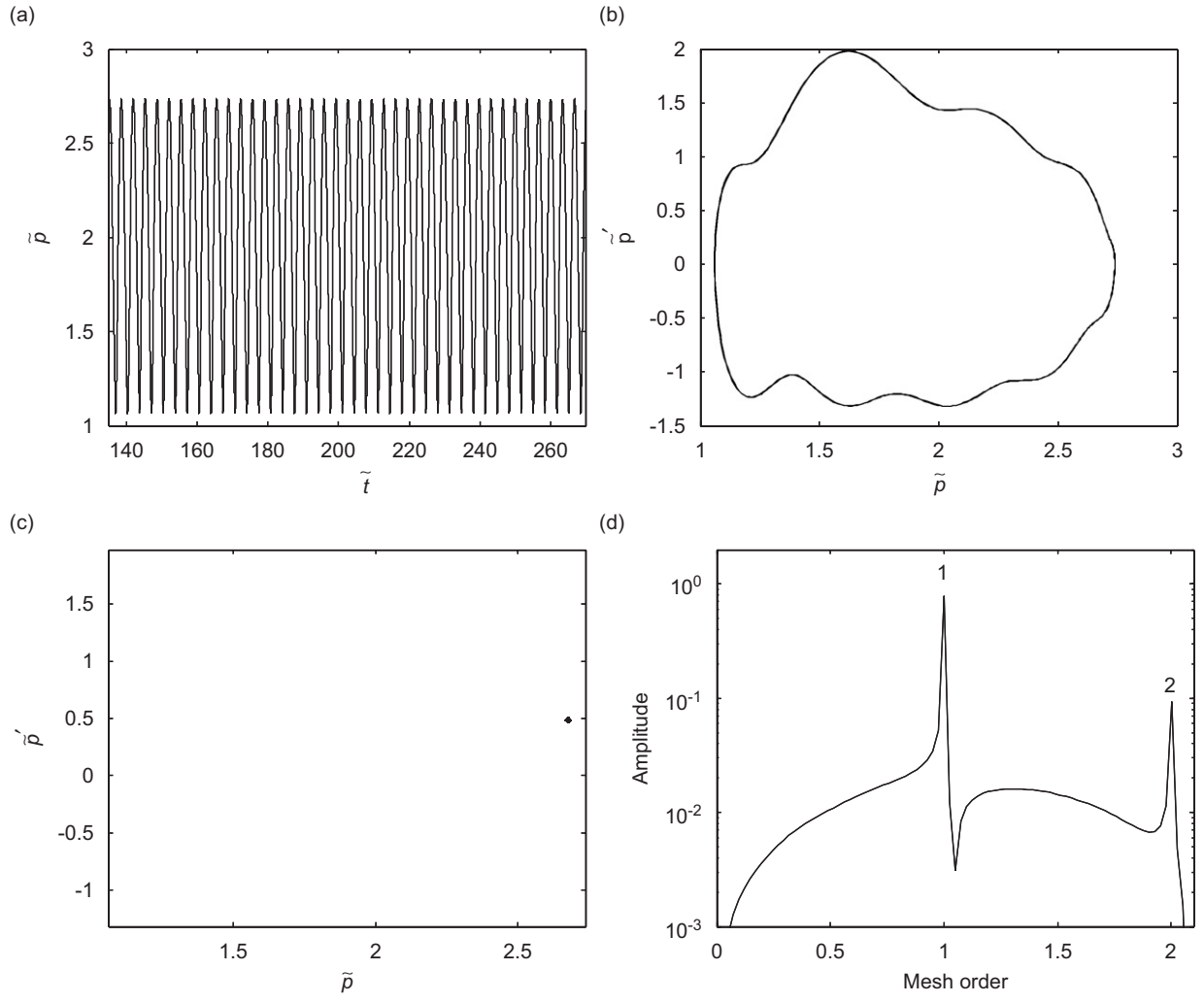

Fig. 23. Period-one response for $\xi = 0.12$, $\tilde{\omega} = 1.8625$: (a) time history; (b) phase plane; (c) Poincare map; (d) FFT spectrum.

4.3.2. Effect of mesh damping on steady-state response

The results of the effect of mesh damping are re-plotted in Fig. 19 to highlight its influence on steady-state response. In Fig. 19(a), the response for lightly damped $\xi = 0.01$ case is shown. In this figure, we can see that several regions are dominated by sub-harmonic, quasi-periodic or chaotic responses. As ξ is increased to 0.03, sub-harmonic, quasi-periodic or chaotic responses can be found only in a region at high frequencies. For $\xi = 0.06$ and 0.12, there are only period-one steady-state responses over the entire frequency range of interest. The effect of mesh damping on frequency response can be seen more clearly by examining the predicted data in other forms like in the above mean load parametric analysis.

The time history function, phase plane plot, Poincare map and FFT spectrum plots of the steady-state responses at $\tilde{\omega} = 1.8625$ for numerous mesh damping values are compared in Figs. 20–23. As shown in Fig. 20, for $\xi = 0.01$ chaotic response is obtained. Time history is non-periodic, Poincare map contains as many discrete points as the number of periods used in the dynamic analysis, and FFT spectrum depicts broad band characteristic. Fig. 21 for $\xi = 0.03$ shows period-six sub-harmonic response. The time history possesses a period equal to $6T$, Poincare map has six discrete points, and FFT spectrum contains peaks at mesh orders equal to multiples of 1/6 in addition to orders 1 and 2. Figs. 22 and 23 for $\xi = 0.06$ and 0.12 show period-one responses where their time history functions have a period T, Poincare map shows one discrete points, and FFT spectrum contains peaks only at mesh orders 1 and 2. Here, it is shown that when mesh damping ratio is increased, the initial chaotic response at $\tilde{\omega} = 1.8625$ progressively transforms into period-six subharmonic response, and subsequently period-one response.

5. Concluding remarks

A general NLTV torsional vibration model of a hypoid gear pair is proposed which considers backlash nonlinearity and time-dependent mesh point, line-of-action, mesh stiffness and kinematic transmission error. The theory is also applicable to spur, helical, spiral bevel gears and worm gears even though the focus here is primarily on hypoid gear. Mesh parameters are first expressed in the fundamental harmonic form to study the effects of their variations on tooth impact regions, dynamic response and the interactions between them and backlash nonlinearity. In this study, the effects of pinion and gear directional rotation radius variation and its interaction on backlash nonlinearity are investigated for the first time. Other important parameters like mean load and mesh damping, are also examined. It is shown that an increase of mean load, mesh damping and system parameter η, and a decrease of mesh stiffness variation, directional rotation radius variation and kinematic transmission error variation will decrease the degree of gear backlash nonlinearity effect. Mesh damping, system parameter η and kinematic transmission error variations affect lightly loaded cases more than heavily loaded ones, while mesh stiffness variation and directional rotation radius variations affect heavily loaded cases more than lightly loaded systems.

Secondly, a new exact time-varying coupling mesh model is proposed which can describe hypoid gear mesh characteristics more accurately and thus is expected to yield a better prediction of dynamic response. It is applied to subsequent dynamic analysis and the effects of mean load and mesh damping on tooth impact and steady-state response have been examined. Numerous nonlinear behaviors such as jump discontinuities, sub-harmonic and chaotic responses are observed, especially for lightly loaded and lightly damped cases. The results show that mean load and mesh damping are two key factors determining the conditions for tooth impact behavior, and subharmonic and chaotic responses.

The proposed single-dof NLTV model will be extended to a higher-dof model to better describe the hypoid gear pair dynamics. Also, the stability of steady-state responses will be analyzed in the future.

References

[1] H.N. Ozguven, D.R. Houser, Dynamic analysis of high speed gears by using loaded static transmission error, *Journal of Sound and Vibration* 125 (1988) 71–83.

[2] H.N. Ozguven, D.R. Houser, Mathematical models used in gear dynamics—a review, *Journal of Sound and Vibration* 121 (1988) 383–411.

[3] R.J. Comparin, R. Singh, Non-linear frequency response characteristics of an impact gear, *Journal of Sound and Vibration* 134 (1989) 259–290.
[4] A. Kahraman, R. Singh, Non-linear dynamics of a spur gear pair, *Journal of Sound and Vibration* 142 (1990) 49–75.
[5] A. Kahraman, R. Singh, Non-linear dynamics of a geared-rotor bearing system with multiple clearances, *Journal of Sound and Vibration* 144 (1991) 469–506.
[6] A. Kahraman, R. Singh, Interactions between time-varying mesh stiffness and clearance non-linearities in a geared system, *Journal of Sound and Vibration* 146 (1991) 135–156.
[7] M. Amabili, A. Rivola, Dynamic analysis of spur gear pairs: steady-state response and stability of the SDOF model with time-varying mesh damping, *Mechanical Systems and Signal Processing* 11 (1997) 375–390.
[8] E.P. Remmers, Dynamics of automotive rear axle gear noise, *SAE Paper* 710114, 1971.
[9] S. Kiyono, Y. Fujii, Y. Suzuki, Analysis of vibration of bevel gears, *Bulletin of the Japan Society of Mechanical Engineers* 24 (1981) 441–446.
[10] E. Abe, H. Hagiwara, *Advanced Method for Reduction in Axle Gear Noise, Gear Design, Manufacturing and Inspection Manual*, Society of Automotive Engineers, Warrendale, PA, 1990, pp. 223–236.
[11] N. Hirasaka, H. Sugita, M. Asai, A simulation method of rear axle gear noise, *Journal of Passenger Cars* 100 (1991) 1383–1387.
[12] M.G. Donley, T.C. Lim, G.C. Steyer, Dynamic analysis of automotive gearing systems, *Journal of Passenger Cars* 101 (1992) 77–87.
[13] Y. Cheng, T.C. Lim, Vibration analysis of hypoid transmissions applying an exact geometry-based gear mesh theory, *Journal of Sound and Vibration* 240 (2001) 519–543.
[14] T.C. Lim, Y. Cheng, A theoretical study of the effect of pinion offset on the dynamics of hypoid geared rotor system, *Journal of Mechanical Design* 121 (1999) 594–601.
[15] Y. Cheng, T.C. Lim, Dynamic analysis of high speed hypoid gears with emphasis on automotive axle noise problem, *Proceedings of the ASME Power Transmission and Gearing Conference, DETC98/PTG-5784*, Atlanta, GA, 1998.
[16] Y. Cheng, T.C. Lim, Dynamics of hypoid gear transmission with time-varying mesh, *Proceedings of the ASME Power Transmission and Gearing Conference*, *DETC2000/PTG-14432*, Baltimore, MD, 2000.
[17] Y. Cheng, Dynamics of High-speed Hypoid and Bevel Geared Rotor Systems, PhD Dissertation, The Ohio State University, 2000.
[18] X. Jiang, Non-linear Torsional Dynamic Analysis of Hypoid Gear Pairs, MSc Thesis, The University of Alabama, 2002.
[19] H. Wang, Gear Mesh Characteristics and Dynamics of Hypoid Geared Rotor System, PhD Dissertation, The University of Alabama, 2002.
[20] S. Vijayakar, *Contact Analysis Program Package: Calyx*, Advanced Numerical Solutions, Hilliard, OH, 2003.
[21] T.C. Lim, J. Wang, Effects of assembly errors on hypoid gear mesh and dynamic response, *Proceedings of the ASME Power Transmission and Gearing Conference, DETC2005-84638*, Long Beach, CA, 2005.
[22] *MATLAB Version 7.0.1 (R14) Service Pack* 1, The Mathworks Inc., Natick, MA, 2004.